Enhancement of the albedo of low stratus marine clouds. Simulations in a global climate model

Elín Björk Jónasdóttir

Abstract

Anthropogenicgreenhouse gases have become widely accepted as the primary cause of global warming. With increasing emissions rates, warming is set to continue and baring any drastic change in mitigation policies, the rate of warming is also likely to continue to increase. According to the IPCC, the increase in radiative forcing associated with a doubling of pre-industrial CO_2 concentrations is estimated to be 3.7 Wm^{-2}

One method suggested to ameliorate the warming is to increase the effects of short wave cloud forcing (SWCF) via geo-engineering and thus restoring the earth's radiative equilibrium. The short wave cloud forcing has a cooling effect by reflecting solar radiation back into space. Twomey [1977] suggested that by increasing the cloud condensation nuclei in thin to moderately thick clouds the optical depth, and thus the albedo of the cloud would increase.

In this study an earth system model is used to explore the effects of deliberately increasing the cloud droplet number concentrations in low level marine clouds. The effects of such increase on the short wave cloud forcing are examined as well as on the effective radius of cloud droplets. Three different geo-engineering cases are presented and compared to a control simulation.

The results show that adding CDNC in marine clouds have the desired impact on SWCF. Effects are increasing with with rising CDNC. For a perturbation of 375 the changes in SWCF are large enough to counteract the increase in radiative forcing by greenhouse gases. The lower CDNC perturbation of 50 cm^{-3} also produce a moderate cooling effect, without completely counteracting the predicted greenhouse gas radiative forcing.

Acknowledgements

My road to a masters degree has not been traditional in any way. With the spectacular financial collapse in Iceland in the fall of 2008 plans to move our family to Oslo and for me to pursue a degree at the University of Oslo came to a screeching halt. In stead, I tried my best to study from a far, sometimes it worked out quite well, and in other cases not at all. With a full time job as a forecaster at the Icelandic Meteorological Office and two major volcanic eruptions in two consecutive years - right around exams the odds were probably stacking up against me, but with the unwavering support of my husband, Daníel, and our two sons Snorri and Trausti it simply never occurred to me to give up. For that, and everything else they have my deepest love and gratitude.

This thesis is mostly written in a few short weeks that I got off from my work, and to my boss Theodór Freyr Hervarsson, and the ever kind and supportive shift manager, Halldóra Jóna Ingibergsdttir I owe a lot for theyÕre understanding and willingness to comply with my somewhat irregular schedule of Oslo trips. My advisors in Oslo, Jón Egill Kristjánsson and Kari Alterskjær I thank for the patience, guidance and quick response to emails. Halldór Bj´ ornsson my advisor in Iceland for interesting discussions regarding this project and many other meteorological phenomena, as well as the R support and to Helene Muri - many many thanks for not once, but twice saving my sanity and my project with help with NorESM and Hexagon.

My friends, family and sometimes total strangers that have hosted me in Oslo, Gisli and Maria, Angel, Arna, Heidar Ingvi, Vidar and Hanna - thank you ever so much. I hope I can repay you someday. Knowing what I know now, I'm not sure I'd do it all again, but I am glad I stuck with it the first time around.

> I've looked at clouds from both sides now, from up and down and still,
> somewhow it's cloud illusions I recall, I really don't know clouds at all.

-Both Sides Now, Joni Mitchell.

Contents

List of Figures

Chapter 1

Introduction

Anthropogenic release of greenhouse gases has become widely accepted as the primary cause of global warming. With increasing rate of emissions, warming is set to continue and baring a drastic change in mitigation policies the rate of warming is also likely to increase. In the fourth assessment report of the IPCC (2007) the equilibrium climate sensitivity, i.e. the warming resulting from the doubling of the concentration of greenhouse gases (measured in equivalent CO_2 concentration) from pre-industrial values, is estimated to be in the range of 2 to 4.5 °C with 3°C being the most likely value [Meehl et al., 2007]. The release of greenhouse gases into the atmosphere causes an imbalance in the radiative budget of the planet. Such imbalance, natural or anthropogenic is referred to as radiative forcing. The change in radiative forcing associated with the doubling of equivalent CO_2 concentrations was estimated by the IPCC in 2001 to be 3.7 Wm^{-2} [Ramaswamy et al., 2001]. As the international agreements to reduce greenhouse gas emissions have not yielded significant emission reductions, alternative methods to reduce the rate of global warming have been seriously considered. In this study one such method based on the idea of deliberately altering low level marine clouds to restore radiative equilibrium is explored, using a earth system model.

Clouds are important in the radiative balance of the earth. The reflection of solar radiation due to clouds produces a negative effect on the radiation budget and is referred to as *short wave cloud forcing*.The interception of long wave radiation by clouds, or *long wave cloud forcing* has a warming effect. Net effects of clouds on the radiative equilibrium are negative and corresponding to global annual average of -13 W/m^2 [Ramanathan et al., 1989] and [Latham et al., 2008]. Radiative and cloud forcing are further discussed in chapter 2.

Twomey (1977) found that by increasing the concentration of cloud condensation nuclei (CCN) in thin to moderately thick clouds the optical depth of the cloud

would increase. Optical depth (τ) and albedo (α_c) of clouds are related variables, and with increased optical depth the albedo increases. Although Twomey's theory was based on the influence of pollution on the albedo of clouds the same principle is used in this study as well as other studies regarding the same topic. In this particular study the actual composition of the CCN is not a factor. For definitions of optical depth and cloud albedo refer to chapter 2.

The optical thickness for any depth of cloud is a function of cloud droplet number concentration (CDNC). With increased CDNC the optical thickness increases. An example of Twomey effects can be seen on satellite imagery, such as figure 1.1 where ship tracks are visible as thicker clouds than the surroundings after the exhaust from the ships have produced new (CCN) in the low marine clouds. The visible tracks in the image are not new clouds, but rather an enhancement of the clouds present when the ship sailed through the area.

In this study the main focus is to increase the natural CDNC count (N) in marine clouds by a fixed number(ΔN). The increase is added on to the natural CDNC count already in the model, and is only done over oceanic areas. The model used was the NorESM, the Norwegian Earth System Model and the experiments run were

1. A control run, without any modifications to cloud droplet number concentration (CDNC)
2. A run where CDNC is increased by 50 per cm^3
3. A run where CDNC is increased by 375 per cm^3
4. A run where CDNC is fixed to a value of 375 per cm^3

Chapter 2 contains the theoretical background of the earth's radiative balance, cloud physics and the physics of low clouds. In chapter 3 discussion of the model and the specifications of the model runs are discussed. A discussion on analysis of the produced data and results is in chapter 4 and chapter 5 includes summary and conclusions.

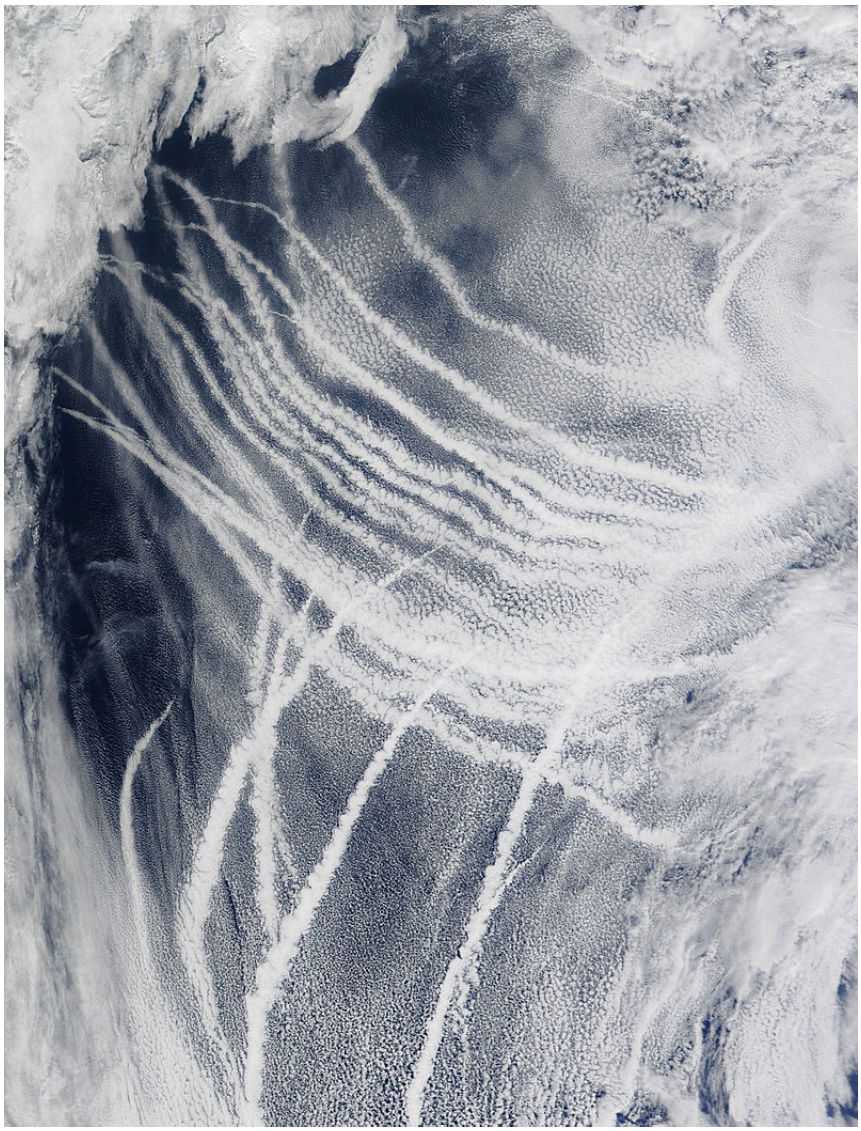

Figure 1.1: A satellite image from NASA satellite Terra showing visible ship tracks in low marine clouds over the North Pacific Ocean on March 4th 2009. The visibly thicker clouds are the result of cloud seeding via ship exhaust in the low marine clouds.

1.0.1 Geoengineering

Deliberate seeding of clouds to enhance albedo is a discipline that belongs to a more general discipline of geo-engineering. By definition from the Special report of the of the Royal Society on geoengineering [2009] the definition is:

> The large scale intervention in the Earth's climate system, in order to moderate global warming.

Strong debate is currently going on regarding whether geo-engineering or climate engineering is justifiable, and to what extent [Schmidt et al., 2008]. Several different methods and technologies have been suggested to counteract global warming. These methods are mainly of two categories, Solar Radiation Management (SRM), and Carbon Dioxide Removal (CDR).

Carbon dioxide removal methods

Methods focused at the root of the problem, to remove greenhouse gases from the atmosphere are referred to as CDR. By decreasing the concentrations of greenhouse gases in the atmosphere there is a subsequent decrease in long wave greenhouse forcing. Methods that involve CO_2 removal or sequestration are e.g. air capture of CO_2 from ambient air, enhanced carbon storage or sinks, both in the oceans and land and the use of biomass for sequestration. Land use management to enhance or protect carbon sinks are also a method of CDR [**?**].

Solar Radiation Management methods

The second category includes projects where the main objective is to reduce the amount of incoming solar radiation that reaches the surface and producing a cooling effect for the planet's climate. SRM methods are mostly methods to treat the symptoms of global warming, but could possibly be useful in emergency such as to avoid reaching a climate "tipping point". [The Royal Society, 2009]. A variety of methods to increase the earth's albedo have been been introduced. The object of this study, enhancement of albedo of low level clouds is one such method. Another method is seeding of the stratosphere, i.e. the injection of large amounts of SO_2 into the stratosphere [Crutzen, 2006]. Sulphate aerosols would accumulate and thus reflect solar radiation at the top of the atmosphere. The effects of injections such as this scheme proposes are analogous to the atmospheric effects of large scale volcanic eruptions. The eruption in Mt. Pinatubo in 1991 and it's effect on climate was closely monitored and may serve as a test case. The effects of increased sulphate in the stratosphere can however increase stratospheric ozone depletion and effect the hydrological cycle and the dynamic effects are not very clear [Schmidt et al., 2008]. Ideas of launching objects such as mirrors in space,

either at a fixed point between the Earth and Sun or in an orbit around the earth have also been discussed. Incoming solar radiation would be reflected away before reaching the atmosphere [Angel, 2006, National Academy of Science, 1992, Pearson et al., 2006].

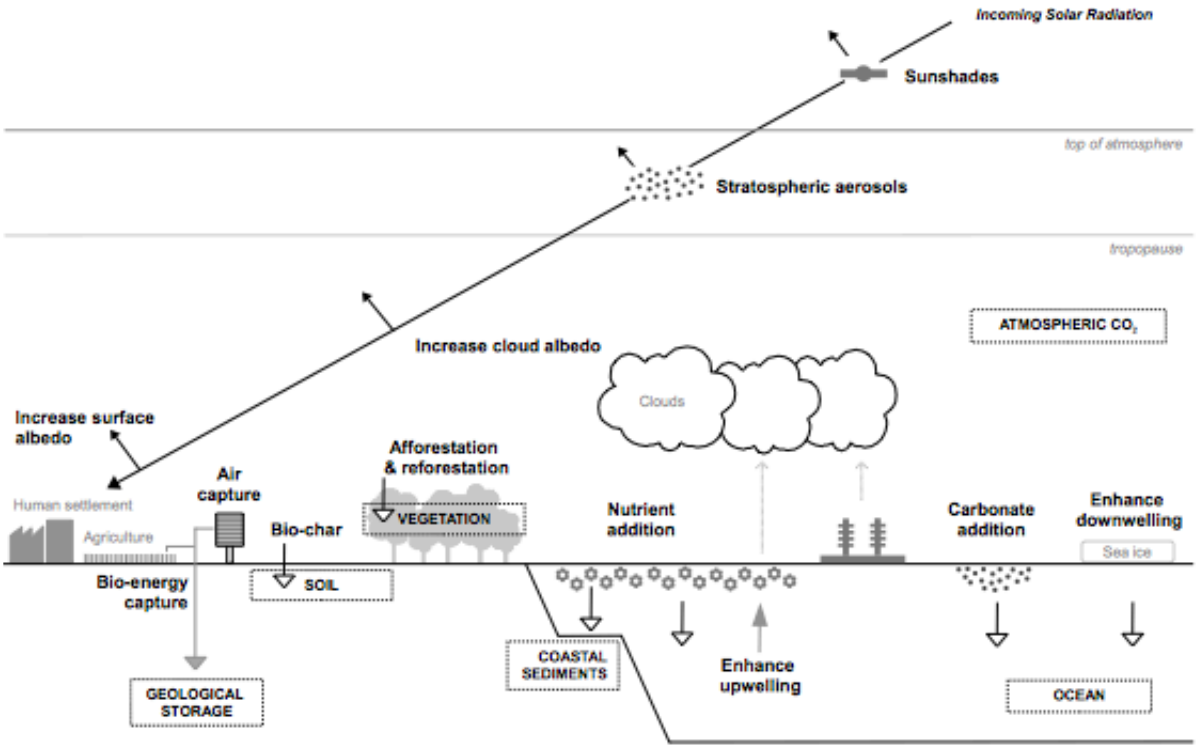

Figure 1.2: A schematic overview of the climate geo-engineering proposals that have been considered by [T.M. Lenton and N. E. Vaughan, 2009]. Black arrowhead indicate shortwave radiation, white arrowheads indicate enhancement of natural flows of carbon, grey downward aero indicates engineered flow of carbon, grey upward arrow indicates engineered flow of water, dotted vertical arrows illustrate sources of cloud condensation nuclei, and dashed boxes indicate carbon stores. From [T.M. Lenton and N. E. Vaughan, 2009]

Increasing low level marine cloud albedo

Latham (1990) presented the idea that by increasing CDNC in natural low marine clouds the effective radius (see equation 2.14) of the cloud droplets would decrease. By increasing the CDNC and decreasing each droplet the combined surface area of the droplets in the cloud would increase and so would the cloud albedo. These effects, i.e. where the increase in CDNC increases optical depth and thus the albedo

(first indirect effect)[Twomey, 1977, Jones et al., 2005] as well as the second indirect effect where the smaller cloud droplets form precipitation less efficiently, and thus give the stratus clouds extended lifetime, increase the local time-mean albedo of the clouds [Albrecht, 1989] and [Jones et al., 2005].

Several studies (e.g. [Slingo, 1990, Kristjansson et al., 2006]) show that to counteract global warming the changes in cloud microphysics such as optical depth, cloud liquid water path (see equation 2.13) and CDNC do not need to be very large to produce a large cooling effect. Kristjánsson et al.,(2005) found that direct and indirect effects of aerosol forcing have negative effects on the radiative balance, i.e. cooling effect. The direct forcing is a term for the increased reflection of incoming solar radiation by aerosols in clear skies, but the indirect forcing comes from the 1st and 2nd indirect effect.

Kristjánsson et al.,(2005) also found the role of climate feedback, "when the result of an initial process triggers changes in a second process that in turn influences the initial one" [Ramaswamy et al., 2001], to be very important. With the main area of increased aerosol forcing was in the subtropics, the largest temperature response was in the northern most latitudes, as well as a southwards shift in the Intertropical convergence zone (ITCZ).

Marine boundary layer clouds are the target for a study such as this one. Low-level single layer stratiform clouds over ocean cover about a quarter of the oceanic surface of the earth [Charlson et al., 1987]. Such surfaces have a surface albedo, α_p of 0.3 to 0.7 on average. Salter et al, (2008) suggested that by using a fleet of unmanned wind driven spray vessels, micron sized drops of seawater could be released into the turbulent boundary layer beneath a marine stratocumulus cloud. This method is not meant to produce new clouds or increase the water vapor content in the atmosphere, merely to activate new CCN to increase the number of droplets in each cloud and therefore increase the cloud albedo.

In the design of vessels the most important aspect is to determine the necessary spray rate of CCN. In the Salter et al., scheme the vessels are wind driven, both in case of movement and the spraying turbine where the vessels sail back and forth perpendicular to prevailing winds and ocean currents. The propellor beneath the vessel moves and creates the electrical energy needed to produce the CCN. Wind is a limiting factor in the positioning of the vessels. Too much wind will hinder production while to little wind will not supply the energy needed to create sufficient power for the vessels. The cost of each vessel in this scheme is estimated to be 1-2 million pounds, which on the global scale of climate change

is considered to be satisfactory. According to Twomey [1977], it is the fractional change of CDNC that drives the change in cloud albedo - and hence Salteter et al, suggest that perhaps spraying into cloud free areas where clouds are predicted to form is the most efficient way of enhancing short wave forcing. The cancellation of 3.7 W m^{-2} associated with positive forcing from the doubling of CO_2 levels [Ramaswamy et al., 2001] will, according to Salter et al, (2008) need a working fleet of 1500 vessels spraying at a rate of around 45 m^3 s^{-1}.

The common practice in previous studies is to increase CDNC uniformly in the marine cloud layer, setting the parameters to a fixed number of CDNC, without regarding the natural, or previous CDNC count [Latham et al., 2008, Rasch et al., 2009, Jones et al., 2009]. This has in fact given results of increased short wave forcing in marine clouds that are previously relatively thin, with low CDNC counts, but in some cases cloud decks off of the continents, especially North America and Asia have been shown to decrease in albedo since pollution acts as CCN, leading to larger CDNC concentrations in the control run than in the run of fixed CDNC. The conclusions to these studies generally show that the relatively inexpensive method of low level marine cloud seeding can be effective as method to increase planetary albedo, albeit only in local areas. In these studies, emission rates of ejected sea salt, wind velocity at the sea surface and other factors were omitted.

Korhonen et al., (2010) simulated a controlled emission of sea spray injections into four areas previously showed to be most susceptible to cloud seeding. They found that the emission rates of sea salt suggested in earlier studies changed the cloud microphysics, but the actual CDNC changes were smaller than previously assumed. The study also indicated that homogeneous spraying of CCN is less reliable than previous studies had assumed and concluded that emission rates and increases in CDNC have to be higher than those assumed in previously in studies such as [Latham et al., 2008] and [Jones et al., 2005].

Chapter 2

Theory

In this chapter the theoretical background of radiative equilibrium and the role it plays in climate and climate change are discussed. In the process general cloud physics is introduced and lastly there is a discussion on low clouds.

2.1 Radiation

Solar radiation drives weather and climate. Solar radiation spectrum covers a wide range of wavelengths, from gamma rays to radio waves[Liou, 2002]. The range of radiation which has wavelengths about from 0.2μm and 4 μm is referred to as shortwave radiation [Hartmann, 1994], this is outside the terrestrial radiation but the earth radiates at wavelengths from about 4μm to 200μ. The terrestrial radiation is thus referred to as long wave radation. Shortwave radiation differs with latitude, season and time of day whereas longwave radiation is dependent on surface type and temperature. The atmosphere is relatively transparent to short wave radiation, much more so than to longwave radiation which means that short wave radiation has easier access to surface than terrestrial radiation has to space.

Temperature and a global average distribution of radiative flux reveals that the net annual radiative flux pattern is close to symmetric between the Southern and Norther Hemispheres, with a maximum at the equator. The solar zenith angle is also a factor in the net radiative flux pattern, and the measurements show that there are gains of radiative energy in the tropics and subtropical regions, but losses in the polar region [Liou, 2002].

2.1.1 Radiative balance

A crude energy balance of earth can be found by considering only the radiative energy fluxes between the sun and earth [Hartmann, 1994]. The net flux of radiative energy though a plane surface can be given as the difference between the incoming shortwave radiation and the outgoing longwave radiation.

$$F_{net} = F_{shortwave} - F_{longwave} \tag{2.1}$$

To determine the net flux at the top of the atmosphere the incoming and outgoing radiation need to be quantified. Incoming radiation varies depending on earths orbital position, but at the mean distance the value give by Harmann [Hartmann, 1994] is

$$S_0 = 1367 W/m^2 \tag{2.2}$$

This value of the solar constant, S_0 the same as the value used by the NCAR CAM4 model, see chapter 3.

The interception of solar radiation by the earth can be viewed as the interception of a disc with the radius of the earth.

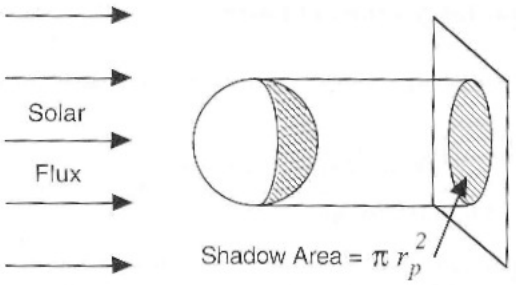

Figure 2.1: Interception of solar radiation by the earth from [Hartmann, 1994], p.25

Absorbed solar radiation (S_a) is calculated by multiplying the solar constant (2.2) by the surface albedo (α_p) and the area of a disk, with the radius of the earth, r_p.

$$S_a = S_0(1 - \alpha_p)\pi r_p^2 \tag{2.3}$$

Outgoing longwave radiation can be found by applying the Stefan-Boltzmann law, which is fundamental to the infrared radiative transfer analysis [Liou, 2002], and multiplied by the surface area of a sphere as the whole sphere of the earth radiates longwave radiation.

$$F_{longwave} = \sigma T_e^4 4\pi r_p^2 \tag{2.4}$$

where $F_{longwave}$ is the outgoing terrestrial radiation, σ is the Stefan-Boltzmann constant and T_e is the emission temperature of the earth. By equating equations 2.3 and 2.4 the emission temperature can be found:

$$F_{longwave} = S_a \tag{2.5}$$

$$4\sigma T_e^4 = S_0(1 - \alpha_p) \tag{2.6}$$

$$T_e = \left[\frac{S_o}{4}\frac{1 - \alpha_p}{\sigma}\right]^{1/4} \tag{2.7}$$

By inserting the solar constant 2.2 and the global mean albedo ($\alpha_p = 0.3$) in to equation 2.7 we find that the earth's emission temperature is close to 255K, but the observed global mean temperature is about 288K. The difference can be explained by natural greenhouse effects. The average incoming solar radiation distributed over the globe is $S_0/4$=342 W/m^2.

Radiative flux (F) at top of the atmosphere is determined by measuring the short wave radiation from the sun (Q), the reflected short wave radiation and the outgoing long wave radiation from Earth [Liou, 2002].

$$F = (1 - \alpha_p)Q - F_{ir} \tag{2.8}$$

On a daily average Q, the insolation can be written as:

$$Q = S_0 \left(\frac{\bar{d}}{d}\right)^2 \cos\theta_s \tag{2.9}$$

where d is the actual distance from the sun, while $\bar{d}$ is the mean distance from which the solar constant is measured and θ_s is the solar zenith angle, the angle between the local normal vector from the surface and a line between a point on the Earth's surface and the sun, see figure 2.2, [Hartmann, 1994]. The net radiative flux can be measured from space, and albedo can be determined by measuring the reflected short wave radiation and comparing it with the insolation. Insolation as well as outgoing long wave radiation (OLR) varies geographically. Measurements also reveal a geographic distribution of albedo.

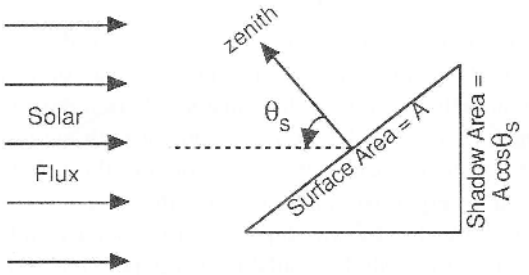

Figure 2.2: Diagram showing the relationship of solar zenith angle to insolation on a plane parallel to the surface of a planet [Hartmann, 1994], p. 29

The greatest flux of OLR is where clouds are scarce and the surface is warm, e.g. in deserts near the equator. OLR flux decreases with increasing latitude since OLR is dependent on the temperature of the surface. OLR flux is also low in the tropics where high and cold cloud tops are dominant. However, outside the tropics the net radiative balance is negative. The maximum insolation and absorption of shortwave radiation is over the oceans near the equator where insolation is high and clouds are scarce so the albedo is very low [Liou, 2002].

Surface albedo is highest where snow and ice cover is greatest and total albedo is highest where both snow and ice are present along with an extensive cloud cover. Specific surface types, such as large deserts also have a high albedo. Surface albedo is lowest over ocean where clouds are sparse. In such areas the total albedo is low. The open ocean without sea ice or cloud cover only has reflectivity of about 8-10 % [Liou, 2002]

The net energy flux at the TOA is positive near the equator where insolation and absorption are high. The energy flux is negative poleward of about 40° N and S, where the solar zenith angle, cloud cover and snow cover all increase towards the poles, and so the total albedo increases whereas the increased solar zenith angle decreases along with insolation and during winter months insolation is very much decreased, if any at all. The atmosphere looses energy to space where the net radiative equilibrium is negative but gains energy where the equilibrium is positive.

2.1.2 Greehouse effect

Greenhouse effects are natural to the earth's atmosphere and play a large role in keeping the global average temperature at 288K. The energy flux between the surface and the atmosphere is larger than the energy flux at the TOA. The magnitude of the long wave energy flux depicts the importance of the greenhouse effects: the larger the flux, the stronger the greenhouse effects [Hartmann, 1994].

In the atmosphere the features that trap outgoing longwave radiation are atmospheric gases that absorb and re-radiate thermal infrared energy and are referred to as greenhouse gases. Among others, greenhouse gases are e.g. water vapor, carbon dioxide and ozone. Greenhouse gases are transparent to shortwave radiation, so while the longwave radiation is trapped in the atmosphere, shortwave radiation is transmitted relatively unhindered towards the surface. When longwave energy is trapped in the atmosphere it acts to bring the system out of radiative balance. However, the absorbed longwave radiation heats the atmosphere and surface, increasing longwave radiation until equilibrium is restored. Figure 2.3 depicts the transfer of incoming solar radiation through the atmosphere. The solid straight arrows are the insolation, which starts out at 100. The dashed straight lines depict the reflected insolation and the curvy arrows represent the transfer of terrestrial radiation from the surface, and the fraction of radiation that gets absorbed and reradiated. Note that the initial value of the outgoing terrestrial radiation is higher than the insolation.

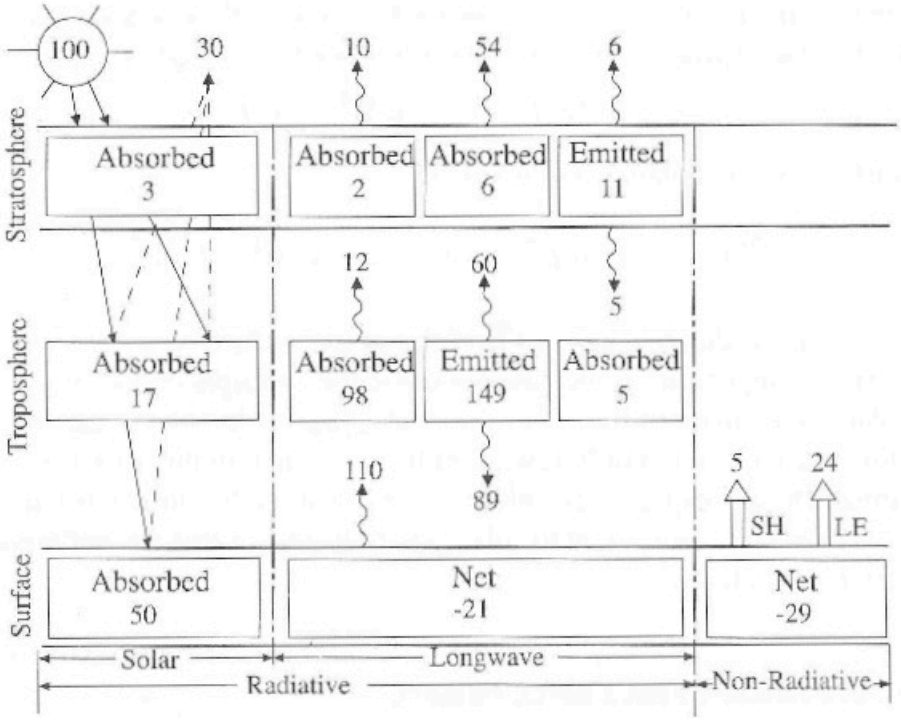

Figure 2.3: Diagram showing radiative equilibrium of the atmosphere [Hartmann, 1994], p. 28

2.2 Clouds

Clouds are important to the radiative balance and global climate. Presence of clouds, water vapor and cloud condensation nuclei (CCN) is ever changing in the atmosphere and cloud patterns converge towards favorable cloud forming sites as well as moving with wind at cloud level [Hartmann, 1994].

When clouds are present they absorb, reflect and/or re-radiate both shortwave and longwave radiation. Clouds thus affect the radiative balance and the temperature of the atmosphere.

A typical satellite image of the earth reveals that organized cloud patterns are present, and they extend for thousands of kilometers in all areas of the world. These patterns are associated with meteorological systems such as low pressure systems, fronts, orographic features and can both stay in place for days or move with prevailing winds. Clouds consist of cloud droplets. They are form by condensation on hydroscopic CCN and lost either by evaporation or precipitation. Clouds

do not consist of the same cloud drops for they're whole life span, but in a system in equilibrium, condensation and evaporation will on average balance. [Rogers and Yau, 1989].

Cloud forcing is a term used to describe the role clouds play in the radiative equilibrium. Short wave cloud forcing (SWCF) is the reflection of short wave radiation due to clouds, while long wave forcing of clouds is comparable to the greenhouse effects where clouds absorb and re-radiate long wave radiation.

Cloud forcing is defined at the TOA as the difference between net downwelling radiation 2.1 in the real atmosphere minus a net downwelling radiation in a hypothetical cloud-free atmosphere with otherwise identical conditions.

$$SWCF = F_{SW,down} * (1 - \alpha_c) - F_{SW,down} * (1 - \alpha_{clr}) = F_{SW,dow}(\alpha_{clr} - \alpha_c) \quad (2.10)$$

SW is the short wave radiation, at the TOA going down into the atmosphere. α_c is the albedo in cloudy (real) atmosphere, while α_{clr} stands for the hypothetical cloud-free atmosphere. SWCF is the shortwave cloud forcing, or the amount of incoming solar radiation reflected back to space by clouds. The values for SWCF are nearly always negative since the total albedo is higher with clouds, than without them, the only exception being polar regions covered with snow and ice. Surface albedo in that case can be equal to or higher than the total albedo with clouds.

The longwave cloud forcing (LWCF) is defined as the difference in terrestrial radiation at the TOA in the cloudy and clear atmospheres.

$$LWCF = F_{LW,up(clr)} - F_{LW,up(c)} \quad (2.11)$$

LW is the longwave or terrestrial radiation, radiating from the earth upwards to the TOA. The variable $F_{up(clr)}$ is the outgoing LW radiation in a cloud-free atmosphere, while $F_{up(c)}$ is the LW radiation outgoing in the cloudy atmosphere. The longwave cloud forcing (LWCF) is the amount of terrestrial radiation the clouds re-radiate or reflect back to earth. LWCF is nearly always positive, because cloud tops are usually colder than the surface and the temperature of the radiating surface determines the OLR. For warm low level marine clouds LWCF is not important because the temperature of the low clouds is very nearly the same as that of earth's surface and the OLR is the same.

SWCF is one measure of the impact of clouds on radiation and climate [Kristiansen and Kristjansson, 1999]. The higher the absolute value of the SWCF, the greater the forcing and the reflection of solar radiation and the atmosphere cools down. [Slingo, 1990].

Forcing of clouds is controlled through the optical depth τ, which is correlated to the cloud albedo α_c. τ is dependent two parameters, the liquid water path (LWP) and the effective radius (r_e).

LWP is the amount of vertically integrated liquid water in a cloud. It can be calculated from the liquid water content (LWC) and the thickness of the cloud [Liou, 2002].

$$LWC = \frac{4\pi}{3}\rho_l \int r^3 n(r) dr \tag{2.12}$$

where ρ_l is the density of water and n(r) is the droplet number concentration in [cm^{-3}]. LWP can thus be found

$$LWP = LWC \cdot \Delta z \tag{2.13}$$

where Δz is the thickness of the cloud.

Mean effective radius of cloud droplets is a variable upon which the calculated reflectivity and transmittance of sunlight is dependent. The mean effective radius differs from the mean radius by taking the droplet cross section into account, and thus the scattering property of spherical droplets. The amount of light they scatter is proportional to their cross sectional area [Liou, 2002].

$$r_e = \int r \cdot \pi a^2 n(r) dr / \int \pi r n(r) da \tag{2.14}$$

where r is the mean radius of the droplets, and r_e is the mean effective radius. We can define the effective radius in terms of optical thickness and LWP [Liou, 2002].

$$r_e \simeq \frac{3}{2\rho_l} LWP/\tau \tag{2.15}$$

By changing these two parameters a change of optical depth and albedo can be brought about.

In thick the insolation is scattered by cloud droplets before it reaches through the cloud and to the surface. The depth within the cloud to which the radiation reaches before it has all been scattered in the cloud is the referred to as the cloud optical depth. Optical depth is the direct controlling parameter of the reflectance of clouds or shortwave cloud forcing [Twomey, 1977]. As cloud forcing is an important factor in the Earth's radiative equilibrium, changing the cloud forcing will have effects on the temperature of the atmosphere. The idea to increase shortwave

cloud forcing - to thicken clouds and thus increase the cloud albedo is an idea first proposed by Latham in 1990. Twomey discusses optical depth as the control factor of cloud albedo and shows how, with increased optical depth the albedo increases.

$$\tau = \int_0^h k_e dz = \pi \int_0^h \int_0^\infty \tau^2 Q_E(\tau/\lambda) n(\tau, z) dr dz \tag{2.16}$$

Where Q_E (τ/λ) is the extinction efficiency given by Mie theory and k_E is the extinction coefficient. For wavelengths in the visible where $\lambda \ll r$,

$$Q_E(\tau/\lambda) \approx 2 \tag{2.17}$$

is adequate [Liou, 2002].

For realistic drop distribution the integration can be eliminated and the optical depth can be reduced to a much simpler formula, [Twomey, 1977]

$$\tau = 2\pi N \tilde{r}^2 h \tag{2.18}$$

N is the drop concentration per cubic centimeter, $\tilde{r}^2$ is the representative mean or model radius and h is the depth of the cloud layer. With large optical thickness cloud albedo can be close to 1, whereas low optical thickness produces clouds with a much lower albedo [Twomey, 1977].

2.2.1 Low marine clouds

Shallow layer clouds such as stratus and stratocumulus have very little vertical motion, and so the condensation of cloud drops can not be accounted for by vertical motion alone. In some areas of the world, specifically over ocean very large persistent sheets of stratus and stratocumulus can be found. Stratocumulus is often seen to partially cover subtropical oceans where the semipermanent subtropical anticyclones dominate the circulation. Stratus clouds can form in large sheets over the Arctic Ocean [Houze, 1993]. When stratus layers form over warm ocean the formation layer is bound by two levels of distinct equivelent potential temperature $(\bar{\theta_e})$. The lower level is near or at the ocean surface and the layer above, generally bound by higher $\bar{\theta_e}$. This is referred to as "cloud-topped boundary layer" heated from below [Houze, 1993]. As the boundary layer over the warm ocean becomes conditionally unstable stratiform clouds form. The clouds can take on the form of stratus or stratocumulus dependent on the strength of the vertical mixing. Figure **??** shows a conceptual model of the formation of stratus clods over warm ocean. The depth of the layer is h. With increasing depth of the boundary layer the tops of the buoyant elements rise above the lifting condensation level (LCL) and form

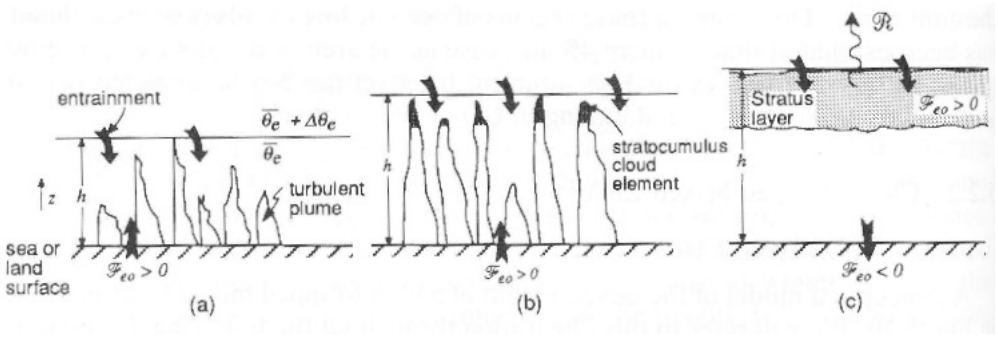

Figure 2.4: A conceptual model of the formation of stratus over warm ocean, within a cloud topped boundary layer. [Houze, 1993]

a small cloud element. As the clouds thicken and form a more continuous sheet of clouds the physical picture changes, and radiation becomes important.

Natural droplet number concentrations N_0 of marine clouds range from 20 to 200 cm^{-3} [Latham et al., 2008]. By implementing Latham's (1990) idea of seeding the low stratus clouds to increase the reflectivity, change in τ and r_e should be detectible. [Twomey, 1977].

Chapter 3

Methodology

In this study the main goal is to run geo-engineering simulations in a earth system model and analyze the effects of increased cloud droplet number concentration on low marine clouds.

By pertubating the cloud droplet number concentrations (CDNC) in warm clouds and comparing the results to a control run as well as a run with a uniform fixed CDNC count the effects of increased CDNC on SWCF and r_e can be estimated. To perform these geo-engineering runs the Norwegian Earth System Model (NorESM) was used. In this chapter there is first an overview of global climate models and NorESM. Next there is an overview of the geo-engineering runs. Data processing and results are disussed in the next chapter.

3.1 Global climate models

General circulation models (GCM) are models used to simulate the general flow pattern of the atmosphere. The first attempts to model the weather with numerical weather models were done in the late 1940's by John von Neumann. Jule Charney lead the first successful numerical weather forecast at the Institute for Advanced Study in Princeton, New Jersey [Hartmann, 1994, Charney et al., 1950]. This first attempt had a model with a single atmospheric layer over the continental United States. In 1956 Norman A. Philips carried out the first successful simulation of the general circulation with a GCM where he mixed the design of a numerical experiment with observations [Lewis, 1998].The progress made in the years following included radiation and dissipation, the equations of motion and increased spatial resolution in both the horizontal and vertical.

Global climate models are complex, they have a dynamical core, which calculates the atmospheric flow by way of the governing equations, as well as a radiation

scheme or core where the moist processes, long and short wave radiation and gravity wave drag are calculated [Mirin and Sawyer, 2005]

State of the art GCMs run with more than one model component, and the meaning of the acronym, GCM has been modified to Global Climate Model. Global Climate models that attempt to forecast the climate response to pertubated climate parameters and in such models the atmospheric component is a part of a larger system of models. Other components in a global climate model are i.e. oceanic modes, ice models, land models and surface models [Hartmann, 1994]

3.2 Norwegian Earth System Model

The global climate model chosen to carry out geo-engineering simulations is the Norwegian Earth System Model (NorESM). NorESM is based on the National Center for Atmospheric Research (NCAR) Community Climate System Model version 4 (CCSM4) [Alterskjaer et al., 2012]

3.2.1 CCSM4 and CAM4

The Community Climate System Model, version 4 (CCSM4) is a general climate model consisting of four different components, each representing a part of the climate system. These components are: atmosphere, ocean, sea ice and land. The components are linked through a coupler that exchanges state information and fluxes between the components [Grent et al., 2011].The first version of the CCSM was released in 1996. It was the first model to maintain stable simulations from the present-day climate without the use of flux corrections. CCSM2 was released in 2002, and CCSM3 in 2004. CCSM4 was released in 2010. The atmospheric component of CCSM4 is the Community Atmospheric Model 4, or CAM4 [Grent et al., 2011]

CAM4 has a Finite Volume (FV) dynamical core. The FV core was developed by scientists at the NASA Godard Space Flight Center in the 1990's [Mirin and Sawyer, 2005] as an alternative to earlier dynamical cores, where finite difference methods or spectral methods were used. Both have limiting characteristics with regard to climate models but the FV core address the issues with both methods, while maintaining a latitude/longitude grid. Discretization of finite volume is local and in physical space. Horizontal discretization is described by Lin and Rood (1996), but the vertical discretization can be referred to as near quasi-Lagrangian [Neale et al., 2010]

The governing equations

The governing equations for the hydrostatic atmosphere are the traditional. They are presented for the 3D atmospheric flow on the sphere for a general vertical coordinate, ζ. All equations are from the Description of the NCAR Community Atmosphere Model (CAM 4.0) [Neale et al., 2010]

The Hydrostatic balance equation, ρ is the density of air, p is pressure, z is the vertical coordinate and g the gravitational constant.

$$\frac{1}{\rho}\frac{\partial p}{\delta z} + g = 0 \tag{3.1}$$

Pseudo-density $\pi = \frac{\partial p}{\partial \zeta}$ is used as a prognostic variable in the conservation of total mass. π is related to the hydrostatic balance by

$$\pi = -\frac{\partial \Phi}{\partial \zeta}\rho \tag{3.2}$$

Where Φ = gz is the geopotential.
The conservation of mass, where $\overrightarrow{V}$=(u,v, $\frac{\partial \zeta}{\partial t}$)

$$\frac{\partial}{\partial t}\pi + \nabla \cdot (\overrightarrow{V}\pi) = 0 \tag{3.3}$$

In a similar fashion the mass conservation law for tracer species can be written

$$\frac{\partial}{\partial t}\pi q + (\nabla \cdot \overrightarrow{V}\pi q) = 0 \tag{3.4}$$

Where q is the mixing ratio of the tracers.
The first law of thermodynamcs, in terms of (virtual) potential temperature Θ

$$\frac{\partial}{\partial t}\pi + (\Theta) + \nabla \cdot (\overrightarrow{V}\pi\Theta) = 0 \tag{3.5}$$

The traditional momentum equations, where (λ, θ) are the latitude and longitude coordinate, A is the radius of the earth, ν is the coefficient for the optional divergence damping and D is the horizontal divergence

$$\frac{\partial}{\partial t}u = \Omega v - \frac{1}{A\cos\theta}[\frac{\partial}{\partial \lambda}(\kappa + \Theta - \nu D) + \frac{1}{\rho}\frac{\partial}{\lambda}p] - \frac{d\zeta}{dt}\frac{\partial u}{\partial \zeta}, \tag{3.6}$$

$$\frac{\partial}{\partial t}v = \Omega u - \frac{1}{A}[\frac{\partial}{\partial \theta}(\kappa + \Theta - \nu D) + \frac{1}{\rho}\frac{\partial}{\theta}p] - \frac{d\zeta}{dt}\frac{\partial v}{\partial \zeta}, \tag{3.7}$$

$$D = \frac{1}{A\cos\theta}\big[\frac{\partial}{\partial\lambda}(u) + \frac{\partial}{\partial\theta}(v\cos\theta)]$$

$$\kappa = \frac{1}{2}(u^2 + v^2)$$

Ω is the vertical component of the absolute vorticity

$$\Omega = 2\omega\sin\theta + \frac{1}{A\cos\theta}\big[\frac{\partial}{\partial\lambda}v - \frac{\partial}{\partial\lambda}(u\cos\theta)\big]$$

ω is the angular velocity of the earth.

CAM4 Physics parameterization is separate from the dynamical core. The parameterization package in CAM4 consist of four components, precipitation processes, clouds and radiation, surface model and turbulent mixing. [Neale et al., 2010] These components are each composed of multiple smaller components, who each parameterize multiple variables. The clouds and radiation component is of interest in this study.

Clouds

Diagnostic methods are used to parameterize cloud fraction in CAM4. The scheme was introduced by Slingo (1987) with numerous variations e.g. Rasch and Kristjánsson, (1998). Three types of clouds are parameterized within the scheme, low-level marine stratus, $\mathcal{C}_{st}$, convective clouds, $\mathcal{C}_{st}$ and layered cloud $\mathcal{C}$. The diagnoses for stratus clouds over ocean in the CAM4 uses

> an empirical relationship between marine stratocumulus cloud fraction and the stratification between surface and 700mb"

[Neale et al., 2010]

$$C_{st} = min\{1., max[0., (\theta_700 - \theta_s) * 0.57 - .5573]\} \tag{3.8}$$

θ_{700} is the potential temperature at the 700 mb level, while θ_s is the potential temperature at the surface.

Radiation

Shortwave and longwave radiation are evaluated every model hour in CAM4 but between the hourly evaluations the fluxes and flux divergences are held constant [Neale et al., 2010].

Insolation at the top of the atmosphere is computed by

$$S_I = S_0 \rho^{-2} cos\mu \tag{3.9}$$

Where S_0 = 1367.0 W/m^2 for a standard configuration.

CCSM4 utilizes the δ Eddington solution as described by Briegleb (1992) to calculate shortwave reflectivity and transmissivity in each vertical layer of the model. The approximation allows for absorption by gases such as O_3, CO_2, O_2 and H_2 O The calculations of aerosols shortwave effects and radiative forcing include the column-integrated optical depth and column-averaged single-scattering albedo, asymmetry parameter and a forward scattering parameter for each aerosol species and spectral interval. The computations are set to zero if the solar insolation is zero [Neale et al., 2010].

Cloud optical properties differ between source areas of droplets. Due to these differences CAM4 has a different parameterization scheme for each of the source area, as well as having separate parameterizations for liquid droplets and ice. For scattering and absorption within clouds the radiative parameterization for liquid water droplets, the method of Slingo (1989) is followed.

The optical properties of liquid cloud droplets are represented in terms of the prognosed cloud water path (CWP), and effective radius, r∇_e

$$r_e = \int r^3 n(r) dr / \int r^2 n(r) dr \tag{3.10}$$

A generalized expression from Slingo (1989) is used for the short wave radiation of liquid clouds. These optical properties are extinction optical depth single scattering albedo, asymmetry parameter and forward scattering parameter. For each spectral interval they are defined:

$$\tau_l^c = CWP\big[a_l^i + \frac{b_l^i}{r_{el}}\big](1 - f_{ice} \tag{3.11}$$

$$\omega_l^c = 1 - c_l^i - d_l^i r_{el} \tag{3.12}$$

$$g_l^c = e_l^i + f_l^i r_{el} \tag{3.13}$$

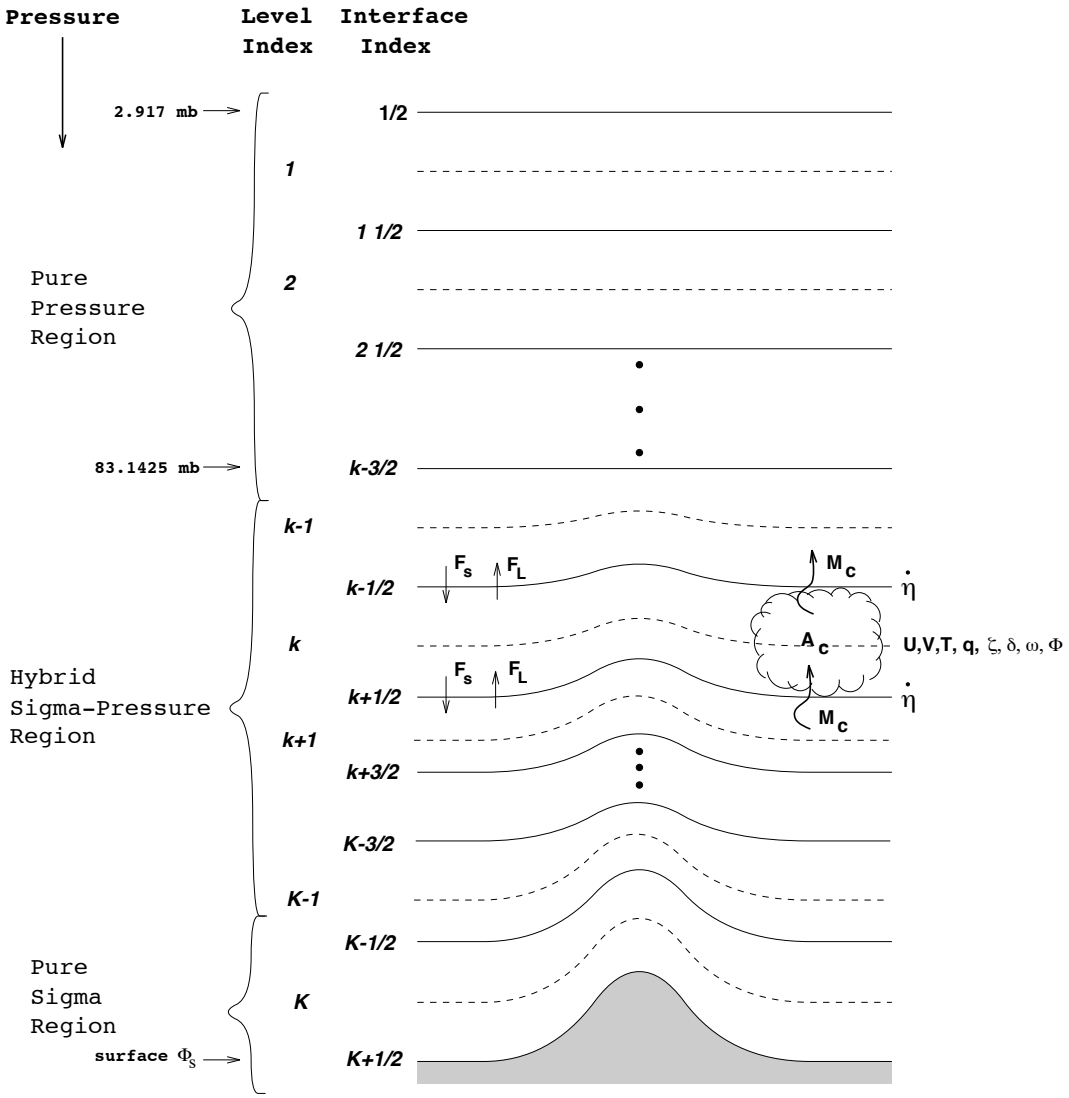

Figure 3.1: The vertical structure of CAM 4.0 [Neale et al., 2010]

$$f_l^c = (g_l^c]^2 \tag{3.14}$$

Longwave solutions are also dealt with within the model. As far as this experiment goes, they are not necessary since longwave radiation is dependent on the temperature of the radiative body and when dealing with low level marine clouds the assumption can be made that the temperature at the top of the clouds is the same, or similar to the temperature at the surface of the planet.

3.2.2 CAM-Oslo

Interaction between aerosol particles, clouds and radiation are a major source of uncertainty in the understanding of mechanisms and the modeling of natural and anthropogenic climate forcings [Seland et al., 2008]. CAM4-Oslo, the atmospheric component of NorESm, has been extended to include a prognostic double-moment cloud microphysics scheme [Storelvmo et al., 2006, 2008] and a detailed aerosol module [Seland et al., 2008]. These modifications allow for the calculations of aerosol indirect effects [Hoose et al., 2009]. A cloud droplet nucleation scheme with parameterized updraft velocities following Morrison and Gettelman (2000) is also an addition to the NorESM, as well as a auto-conversion parameterization following Rasch and Kirstjánsson (1998), [Alterskjaer et al., 2012]. CAM4-Oslo runs at a resolution of 1.9° x 2.6° and 26 vertical levels from surface to about 3,5 hPa.

3.3 Geoengineering simulations and data processing

For the purposes of this study the geo-engineering simulations discussed a few changes were made to the code, and the all the simulations were run offline. An offline run, is a run in which the meteorological forcing and development is the same for all years and the shortwave cloud forcing can be examined without the interference of meteorological noise. The model is run with a fully coupled ocean, a land carbon cycle, but not an oceanic carbon cycle. The runs also use year 2000 greenhouse gas concentrations, and year 2000 CMIP 5 (Coupled Model Intercomparison Project) aerosol emissions. No changes were made to these factors in the simulations.

Chapter 4

Analysis and results

In this chapter the results from geo-engineering simulations are presented. First there is a discussion on the control run of the NorESM, which simulates the current climate. Features important to the analysis of data such as the short wave cloud forcing (SWCF), the distribution of cloud droplet number concentration (CDNC), as well as the distribution and range of size of effective cloud droplet radius (r_e). Each perturbation case is then presented and discussed individually and last the cases are compared and results of the geo-engineering runs compared to the control run to determine the effectiveness of increasing the CDNC in clouds over ocean to increase the shortwave cloud forcing. Summary and conclusions follow in the next chapter.

For each case 7 years of data were produced in a monthly output. For analysis the last 5 years are used. The data is analyzed both in terms of 5 year averages calculated from the monthly output and seasonal average of the same period. Seasonal averages are calculated for each season and are defined as averages of three months producing one season. December, January, February (DJF), March, April, May (MAM), June, July, August (JJA), September, October, November (SON). All runs, both the control and geo-engineering runs are run offline in the earth system model. Offline is simply a way of running a model without a change in the meteorological evolution between years.

4.1 Control run

A control run, or simulation is a run of the model without any changes to the physics of the radiation and cloud schemes. The data from this run simulates the current climate. In the analysis prominent features that are found in the real climate, such as increased availability of cloud condensation nuclei (CCN) over land, be it due to natural or anthropogenic causes is visible. Values from the control run are regarded as base values for the comparison between the control run and the geo-engineered runs.

Figure 4.1 depicts the values of CDNC at around 930 hPa. Prominent features on the map include both high and low counts of CDNC, with the elevated values mostly over land, but the lower values over ocean. A pattern such as the one depicted here is to be expected. CDNC is naturally higher over land where the availability of CCN is greater. CCN is naturally lover over oceanic areas and so the CDNC is lower. Sources of CCN over land can be numerous, pollution, dust, and biological material can all be useful as CCN. On figure **??** prominent areas of elevated CDNC can be found over land in densely populated places, as well as close to natural sources of CCN, such as deserts. Over ocean elevated levels of CDNC can be found on both sides of the continents such as Africa, North and Central America as well as around Australia, and in the Pacific ocean near the equator, although the values are less elevated than over land. Mean value of CDNC in this run is 48,97 cm^{-3} over all pressure levels.

The effective radius of cloud droplets, r_e affects τ and thus the albedo. The premise of Towmey's work is that with increased CDNC the effective radius decreases. By comparing figures 4.1 and 4.2 we can see that in some places of elevated CDNC the r_e is in rather low. In South America there is a high of CDNC, and in in the same location there is a minima of r_e. Note that these graphs at the 930 hPa level. Another similar situation is in Northern America but along the Northwest coast of North America there is a minima in CNDC, but a maxima in r_e. Similar patterns are visible over Asia and Africa. Mean in-cloud r_e is 10 μm.

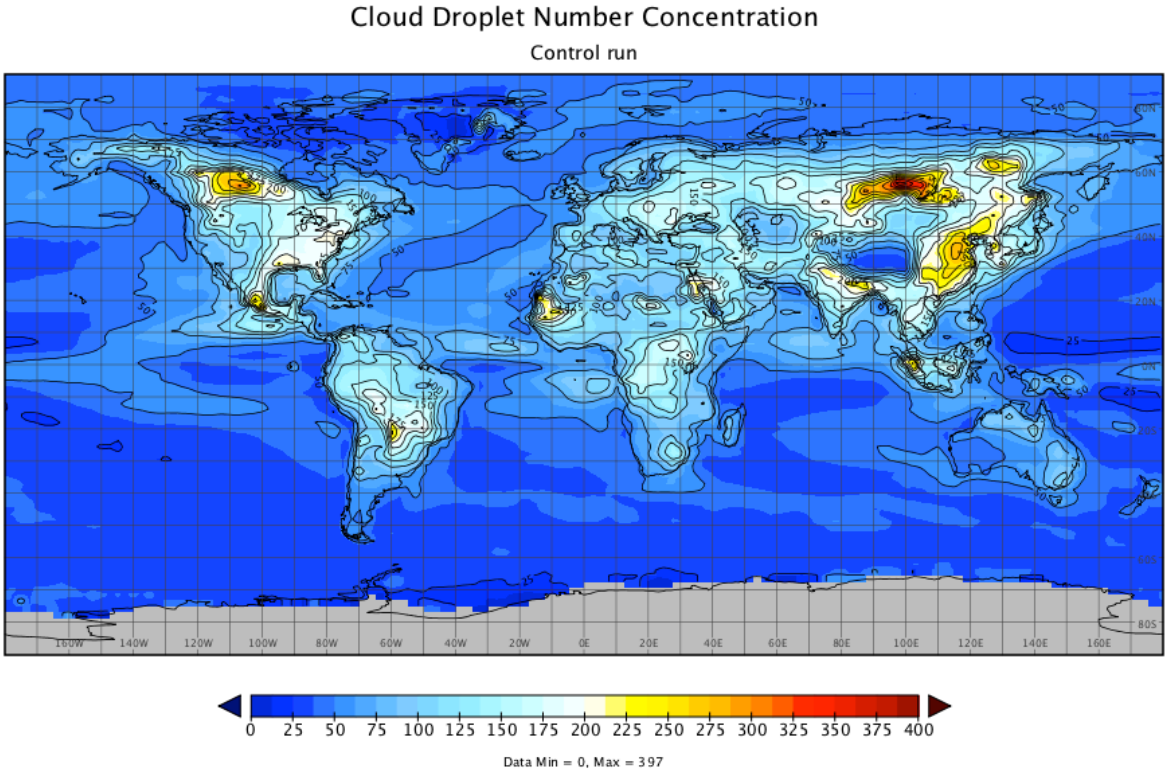

Figure 4.1: In-cloud CDNC, cm^{-3} at 930 hPa

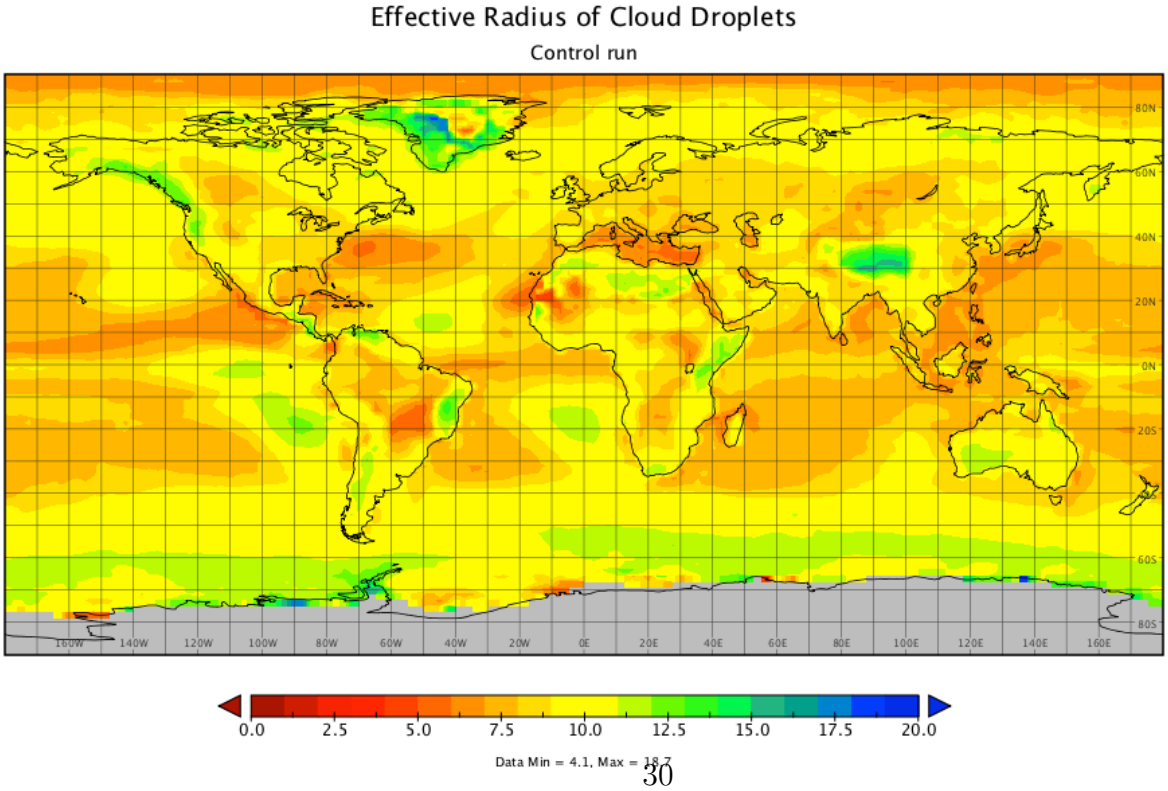

Figure 4.2: Effective radius of cloud drops, r_e in μm

The zonal average of variables can be a useful tool to see changes both in latitudes and the vertical coordinate. For r_e this can be useful, as drop sizes are not uniform in clouds, neither with regard to vertical or horizontal extent.

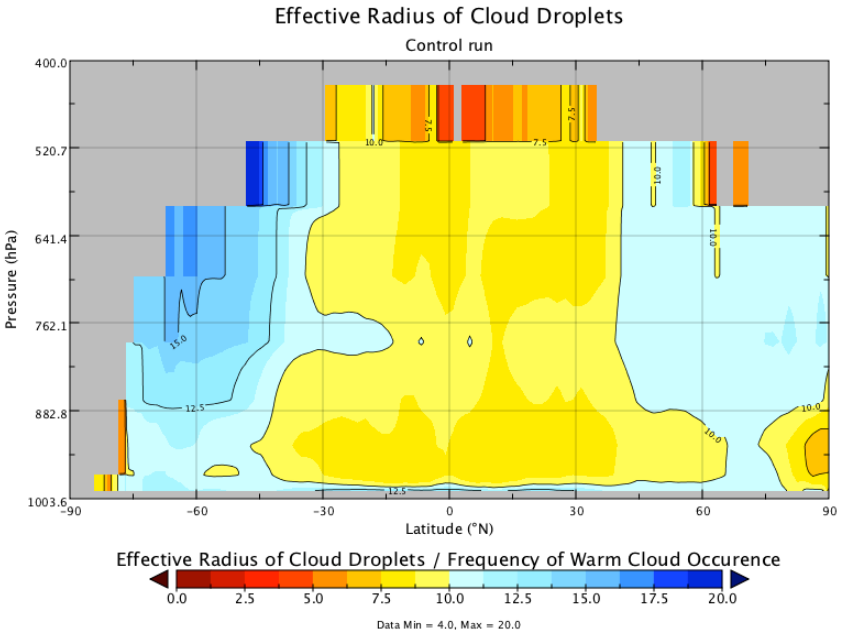

Figure 4.3: Zonally averaged r_e, in μm

Figure 4.3 illustrates a zonal average over both ocean and land from the surface up to about 500 hPa. In this zonally averaged plot the largest drops are evident in the the Southern Hemisphere, between 30°S and 60°S. This area is mostly covered in ocean, but in the same position on the Northern Hemisphere the has a much higher fraction of land. Fewer CCN are available in general in the Southern Hemisphere as much more of the surface is covered in ocean than in the Northern Hemisphere. The availability of CCN in the Northern Hemisphere accounts for smaller droplets while the vast oceans account for the larger drops S of the equator.

Short wave cloud forcing (SWCF) of the control run is depicted in figure 4.4. It clearly shows the difference in SWCF between areas of the world, as well as ocean and land. The mean value of SWCF for the control run is -45.39 W/m^2. The main pattern of SWCF is in some instances similar to the pattern of CDNC, as is to be expected from Twomey's theory. Around the equator in the Atlantic there is a slight increase in the CDNC, and with that the SWCF strengthens. Over Southeast Asia, Indonesia and Malaysia where CDNC increases over land and the

oceanic areas in the vicinity the SWCF also strengthens.

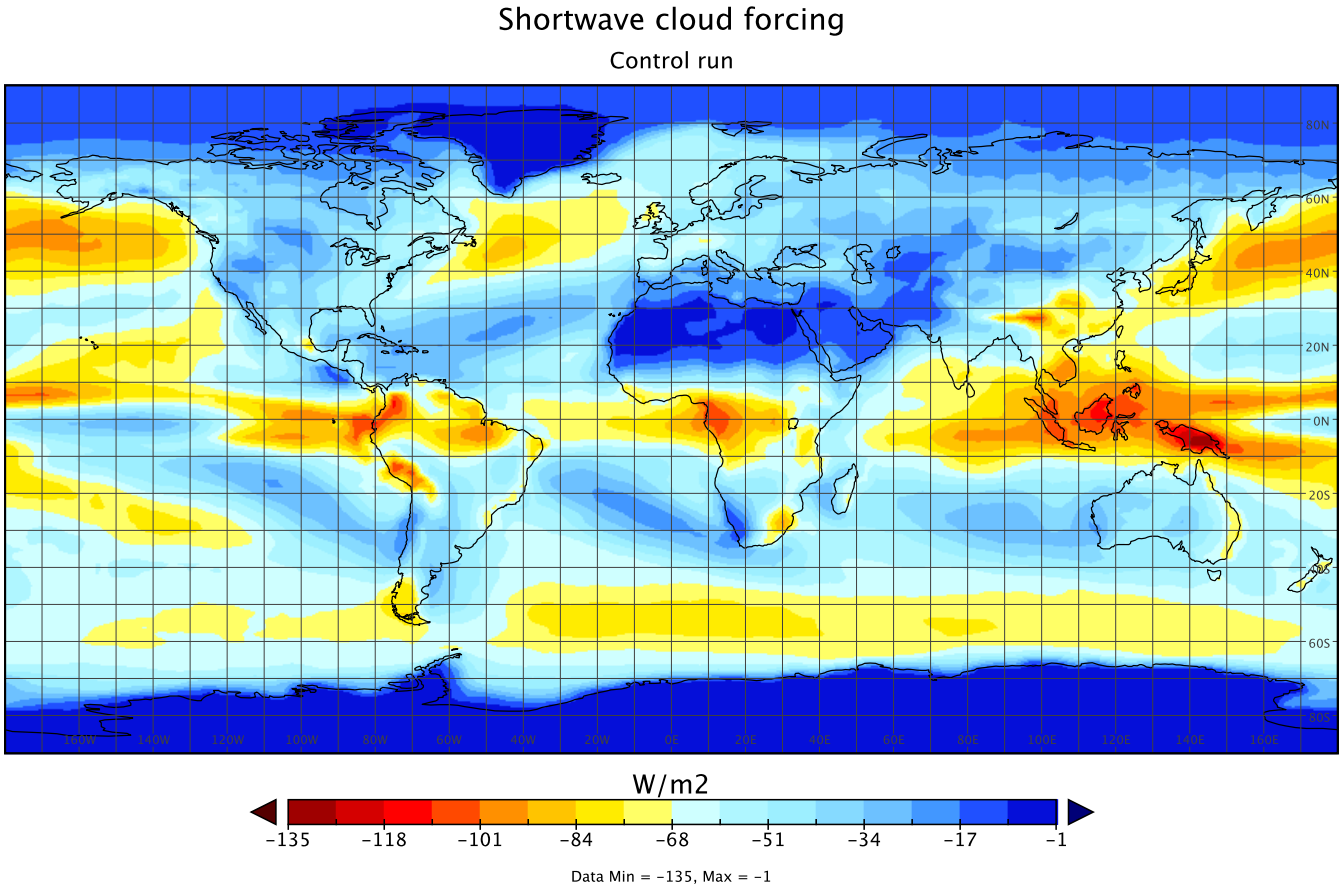

Figure 4.4: Short wave cloud forcing in W/m^2

For general information a plot of the cloud fraction (figure (4.5) at pressure level 930 hPa as well as the cloud frequency of occurence (figure (4.5) is depicted. Since the values of CDNC and effective radius are weighted by the cloud frequency of occurence all values of CDNC and r_e are in-cloud.

Cloud fraction is, at this relatively low level in the atmosphere highest over the ice sheets in the Antarctic and Greenland, but lowest over ocean. The frequency of warm clouds is highest near the equator but decreases in the extra tropics and midlatitudes. Frequency of warm clouds is also significantly less over land than oceans.

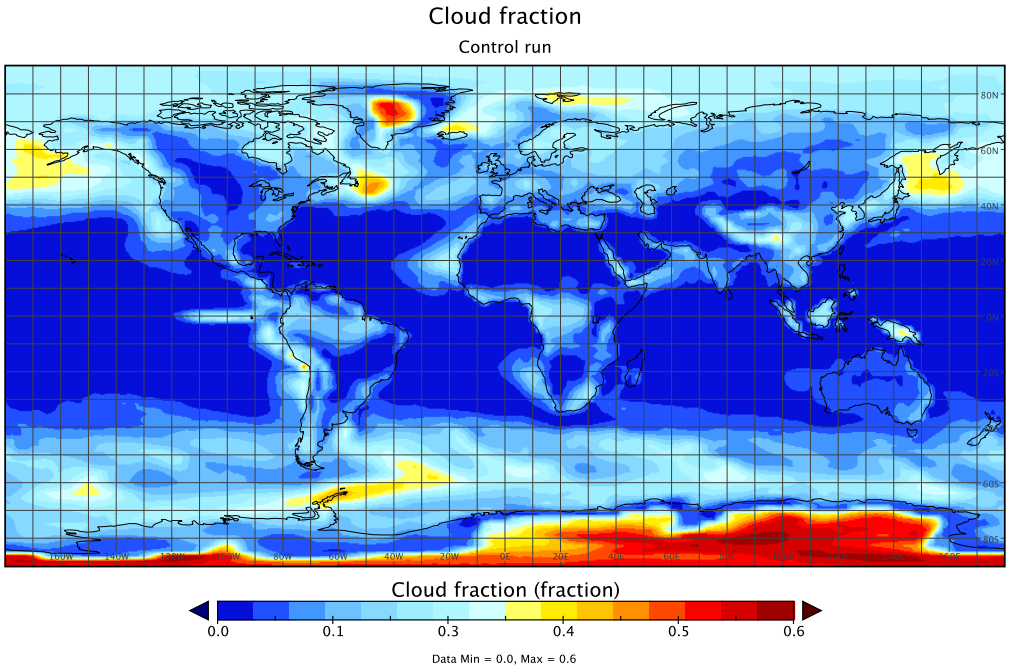

Figure 4.5: Cloud fraction over land and ocean from the control run

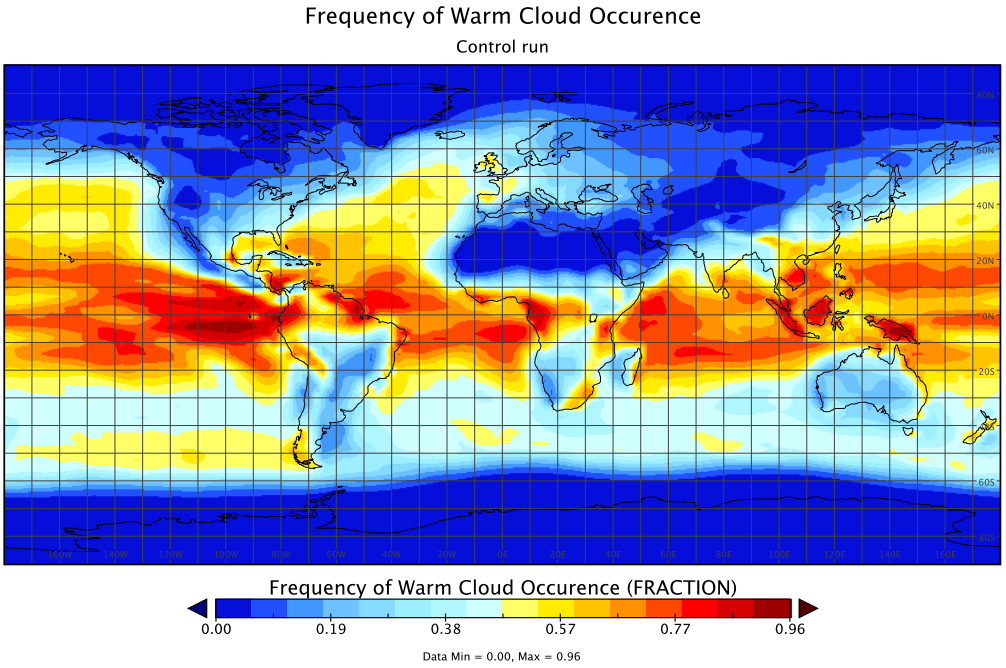

Figure 4.6: Frequency of occurrence over land and ocean from the control run.

4.1.1 Seasonal results

Some variables such as SWCF are dependent on the incoming solar radiation. To become familiar with the difference in the data between seasons results for the control run are also presented in seasonal averages. In figures 4.7 and 4.8 the difference in SWCF with the seasons is evident. There is a clear difference in the strength of the forcing between hemispheres, where the forcing is significantly weaker in the Southern Hemisphere.

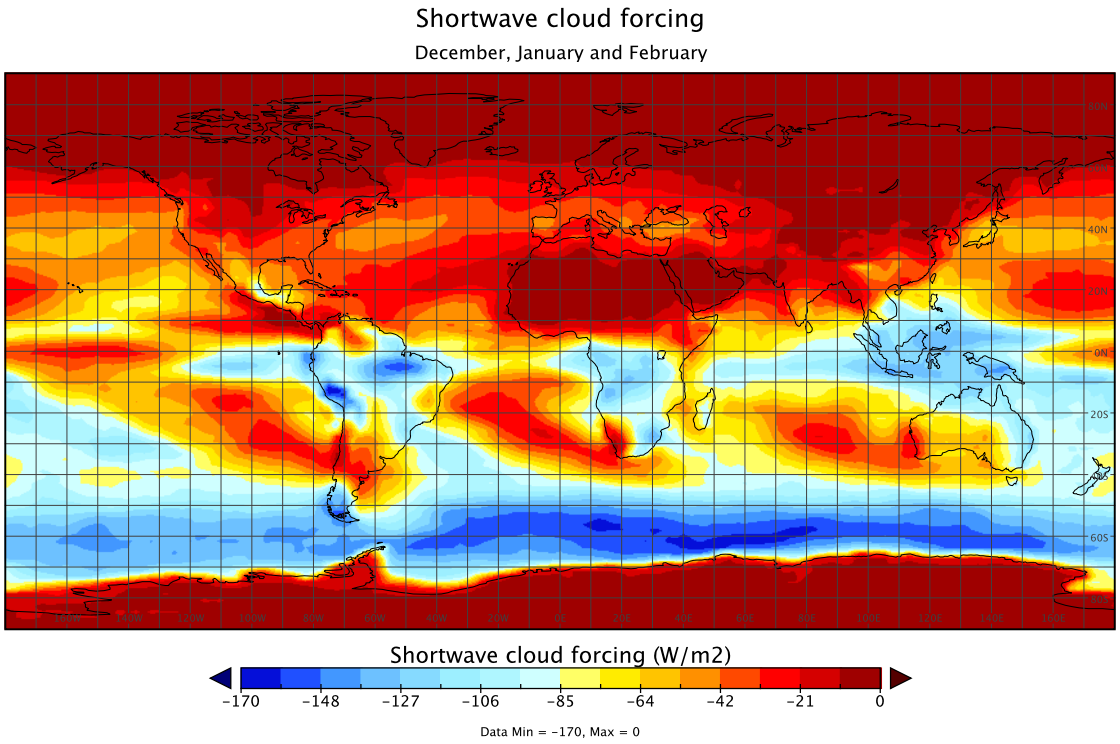

Figure 4.7: Short wave cloud forcing during Nothern Hemispheric winter, W/m^2

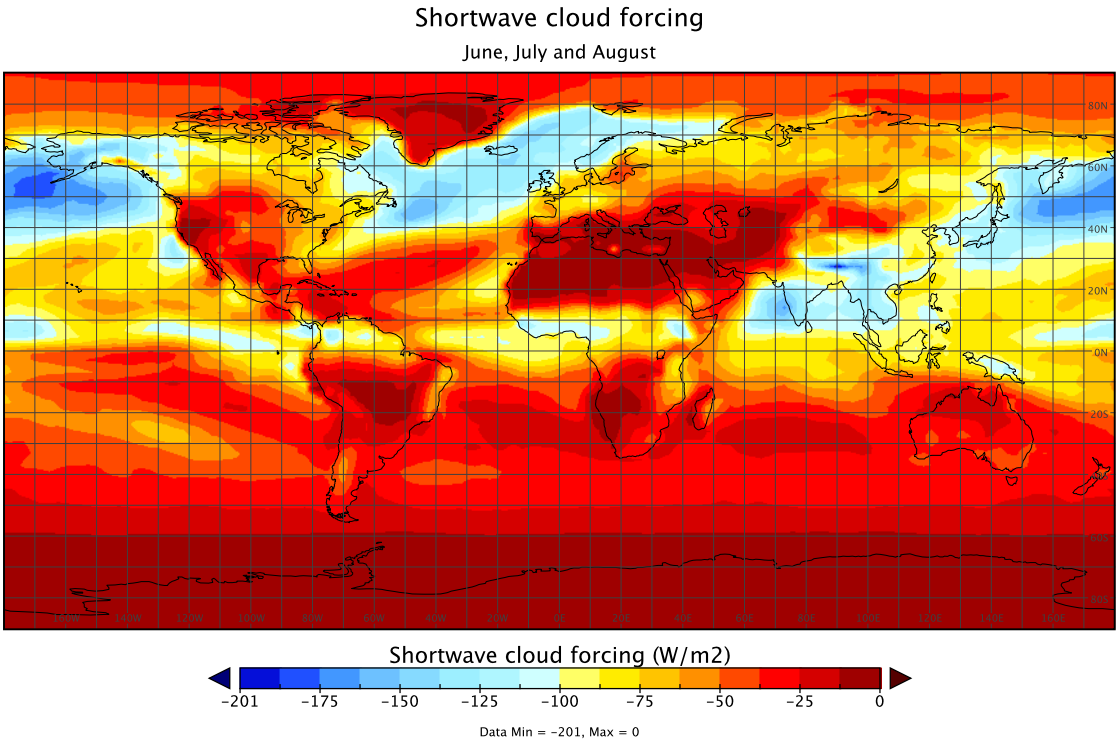

Figure 4.8: Short wave cloud forcing during Nothern Hemispheric summer, W/m^2

4.2 Geoengineering run, N+50

The first geoengineering run was an experiment to add 50 drops to the natural CDNC. The effects to be expected are a decrease in r_e, as well as a strengthening in the short wave cloud forcing. The difference in the mean SWCF between the CNDC+50 and control simulations is -2,5 W/m^2. So the increase in CDNC has a net cooling effect on the system. The mean value of r_e for this run is 8,55μm and the difference in r_e between CDNC+50 run and the control run is 1,52 μm, where the higher values are in the control run.

The zonally averaged distribution of the change in CDNC is plotted in figure 4.9. The largest increase is over the oceans in the Southern Hemisphere, that is to be expected since the geo-engineering is only done over ocean. The change in both r_e and SWCF is largest in the same area.

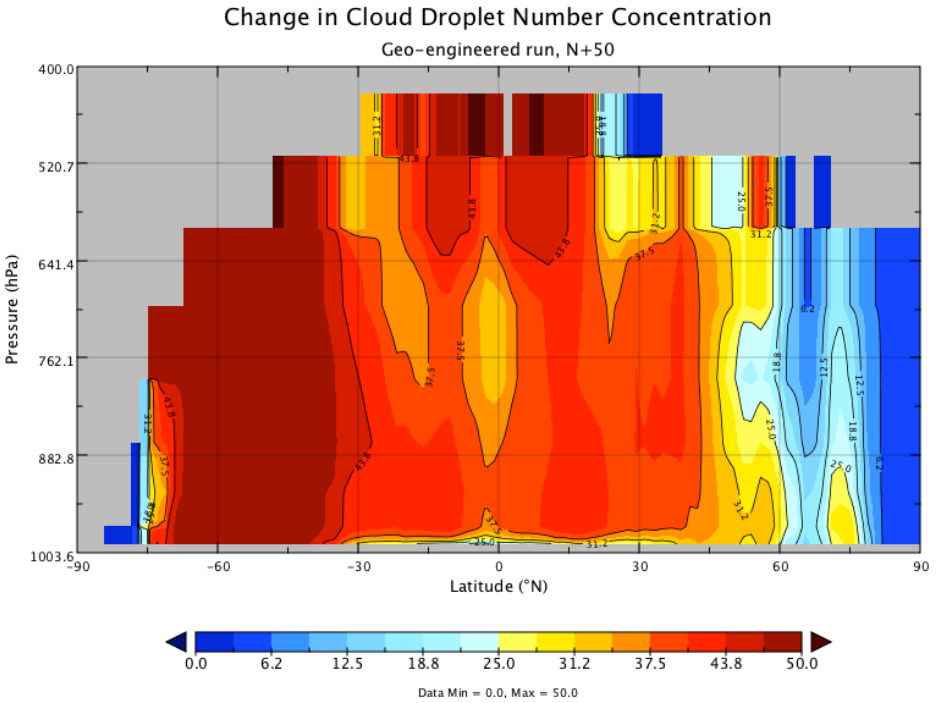

Figure 4.9: Zonally averaged change in CDNC, cm^{-3}

Figures 4.10 and 4.11 represent the zonally averaged difference in r_e between runs and the zonally averaged r_e respectively. The distribution has changed the most in the Southern Hemisphere, and near the equator. Almost no change in r_e

occurred in the regions N of 60N, which is not surprising since both ocean and warm clouds are scarce in that area.

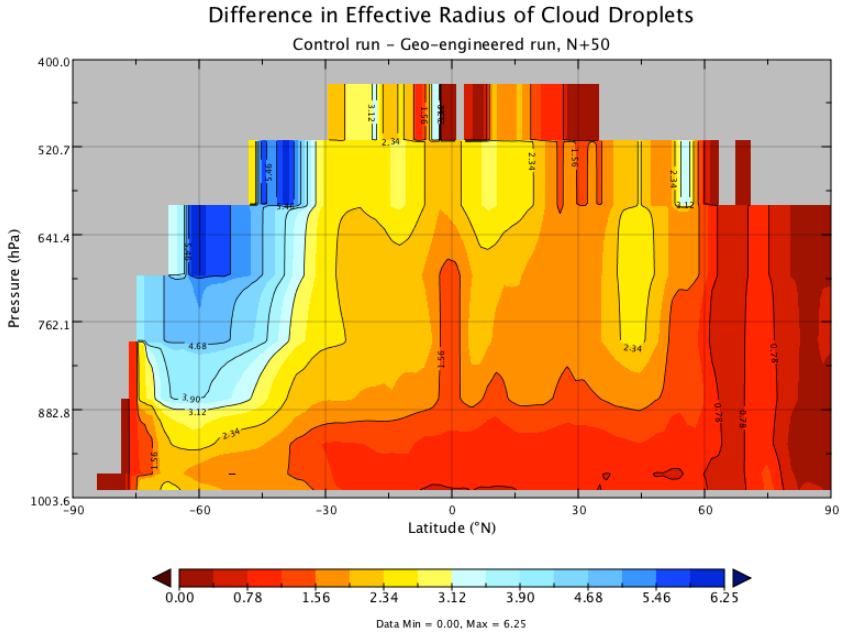

Figure 4.10: Difference in r_e in μm

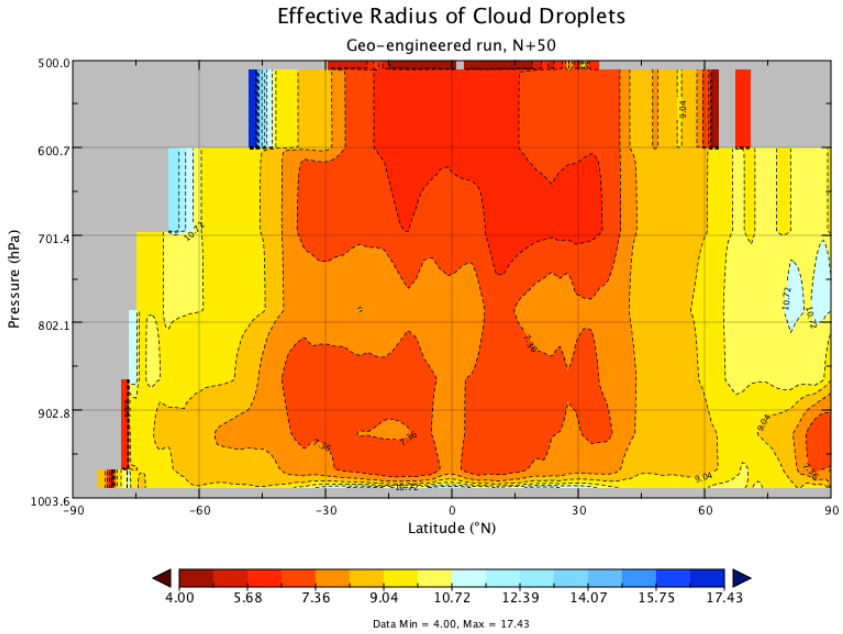

Figure 4.11: Zonally averaged r_e in μm

The change in SWCF between the control run and N+50 run is -2.47 W/m^2 and the mean SWCF in this run is -47.55 W/m^2. The change between the runs is seen in figure 4.12. Areas of the greatest change are around the equator, the most prominent areas in the Pacific Ocean, both north and south, as well as in the Indian Ocean, south of the equator.

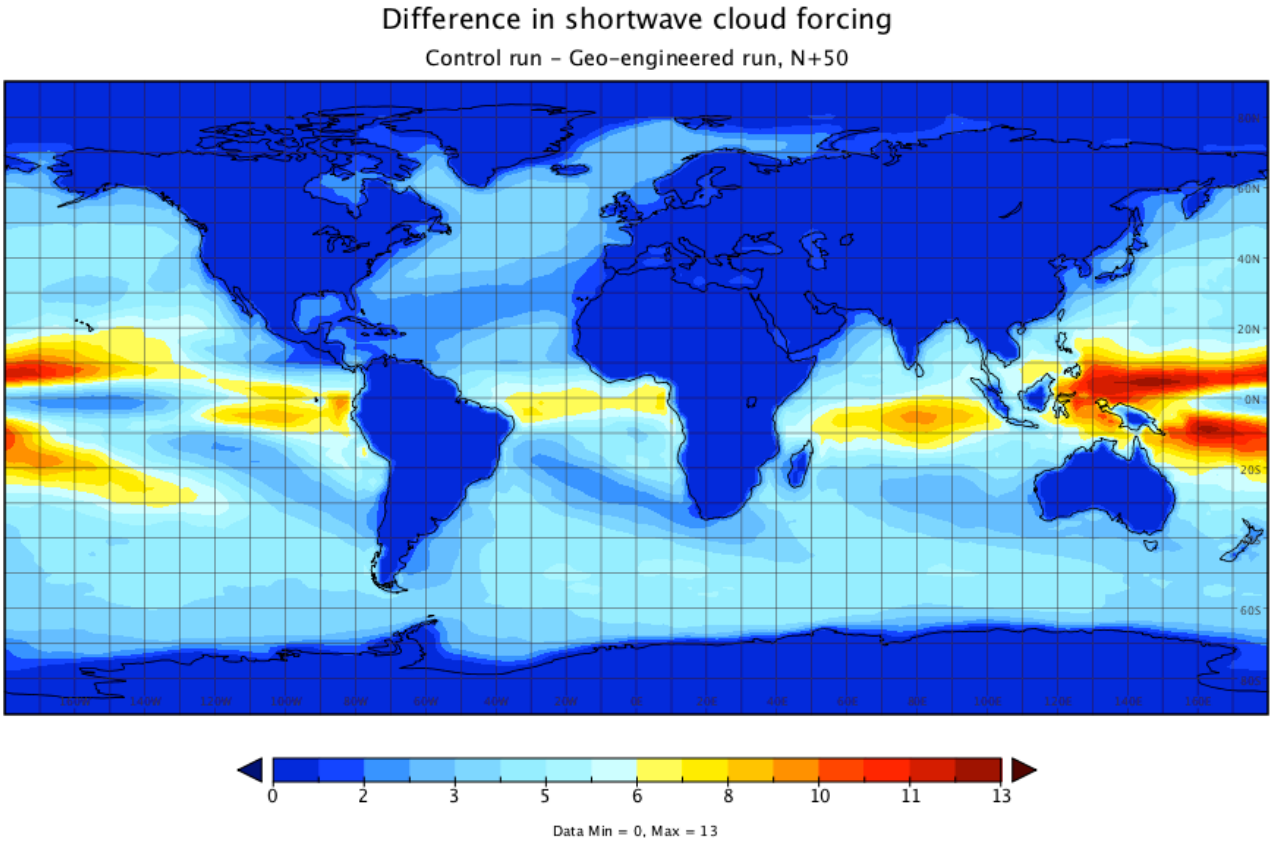

Figure 4.12: Difference between the control run and geo-engineered run in SWCF, W/m^2

4.3 Geoengineering run, N + 375

The work of Latham et al [2008] is in part an incentive for this study. The experiment carried out in that study was set up so that all values of CDNC in low level maritime clouds were set to 375 cm^{-}3. Here, in order to allow for comparison between the studies two experiments with this particular incase are conducted, the first to add 375 cm^{-}3 to the CDNC in warm clouds, the second to set the CDNC to a fixed number of 375 cm^{-}3. The reason for the two different experiments is that the problem with uniform CDNC count in all clouds over ocean is that is is not practical, and secondly it can produce a warming effect since there are clouds likely to have higher concentrations of CDNC already.

In figure 4.13 the pattern of the distribution of CDNC differs somewhat from the control and N+50 runs as.The largest values are now over the largest oceans in the Southern Hemisphere, very much different from the previous runs.

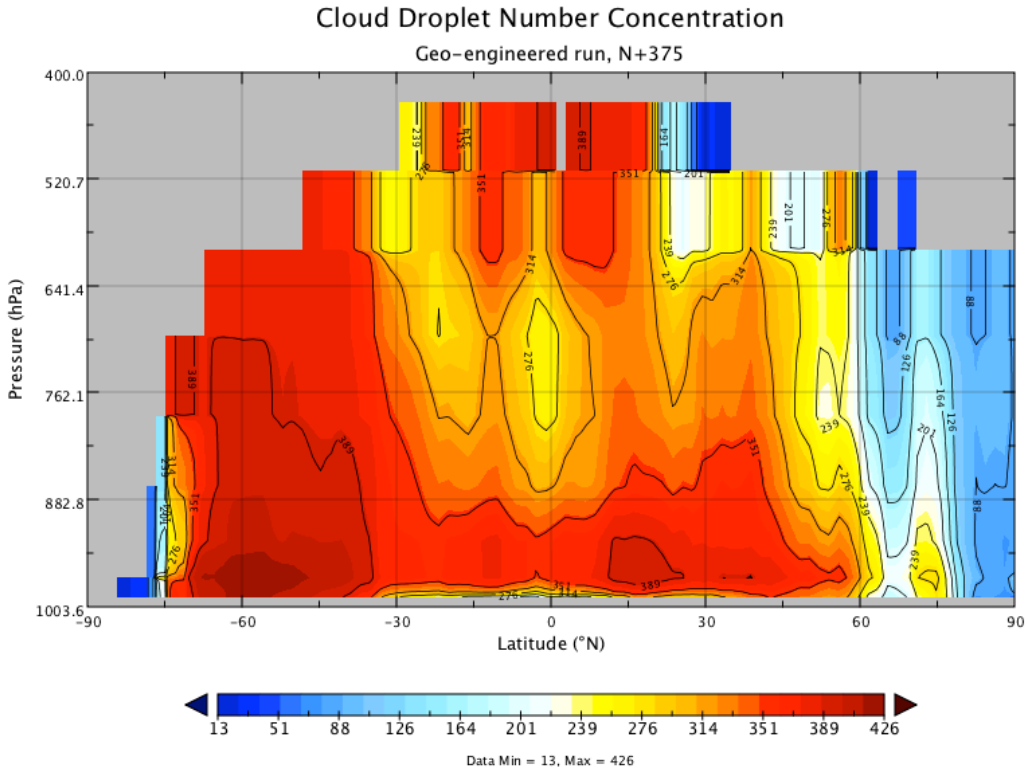

Figure 4.13: Zonally averaged CDNC, cm^{-3}

The pattern in figure 4.14 is very much the same as before, and in this case rather similar to the distribution of total CDNC (figure 4.13).

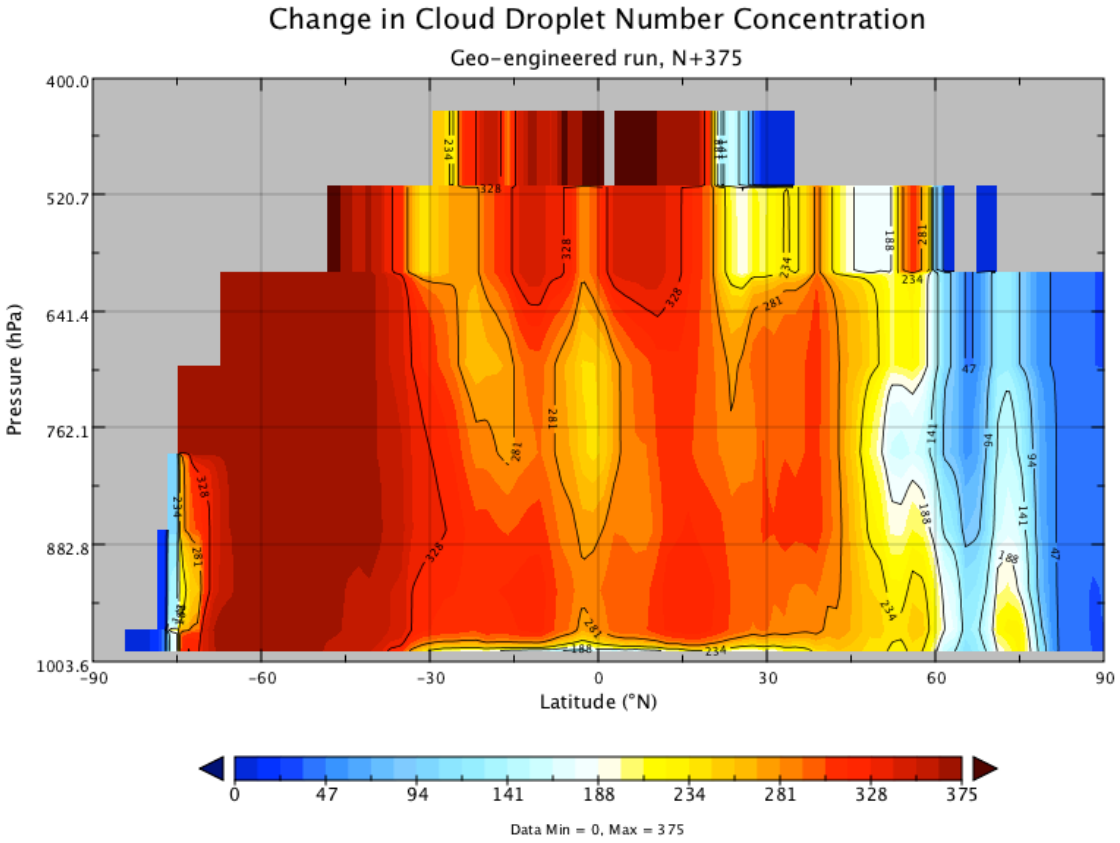

Figure 4.14: Zonally averaged change in CDNC, cm^{-3}

Change in r_e from the control run is much more pronounced than in previous geo-engineered run. The values are mostly lower than 10 μm and in many cases lover than 8 μm. See figure 4.15. The mean r_e is 7,28 μm compared to 10μm in the control run. The distribution of the change is not surprising, and follows the pattern already established.

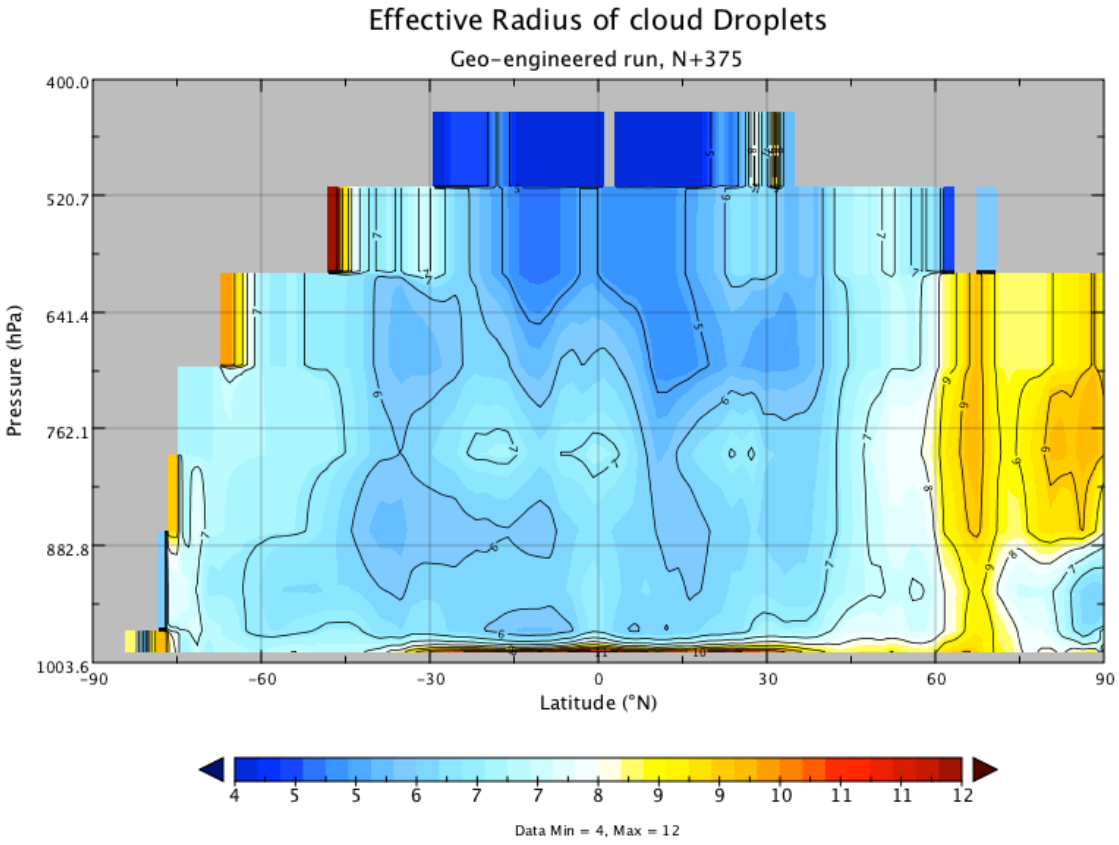

Figure 4.15: Zonally averaged CDNC, cm^{-3}

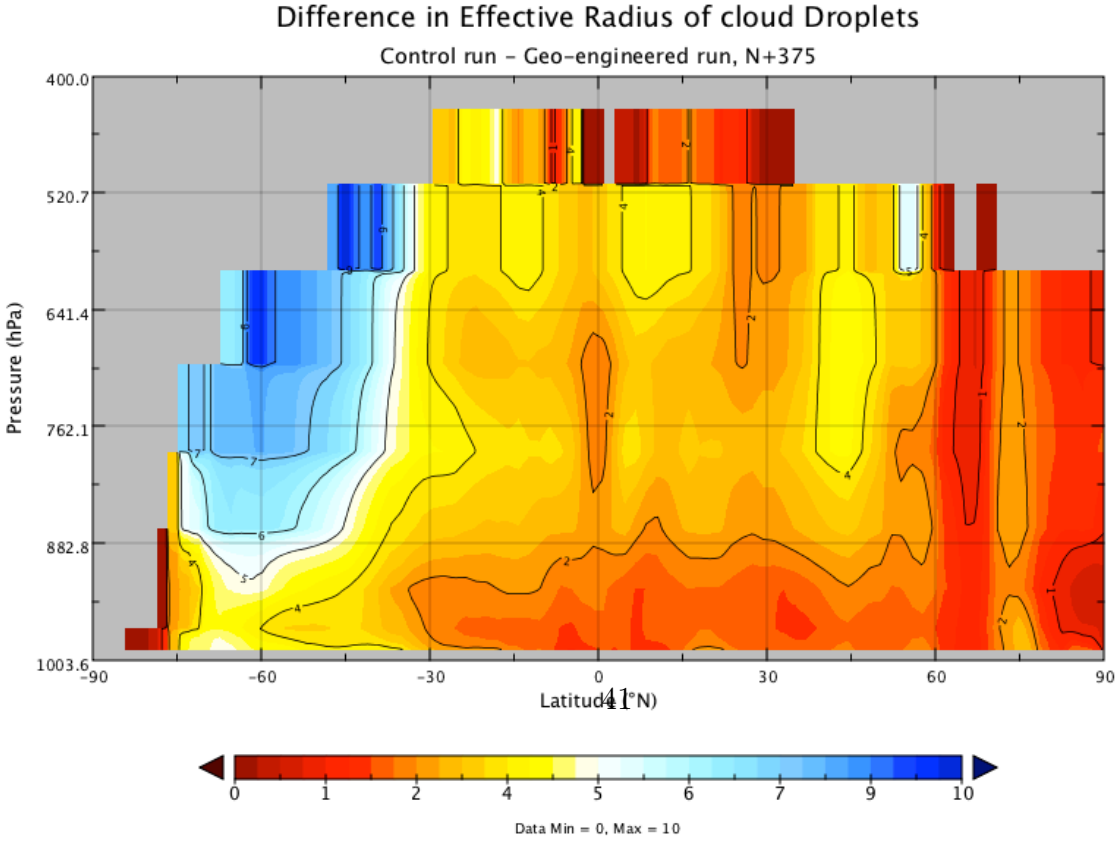

Figure 4.16: Zonally averaged difference in CDNC, cm^{-3}

The mean SWCF is -50,35 W/m^2. The change from the control run is - 4,96 W/m^2. The difference between the two runs is depicted in figure 4.17. The pattern of the strengthening of the SWCF keeps to the same general area and does not divert much from the areas in the North and South Pacific, and the Indian Ocean but becomes somewhat more prominent.

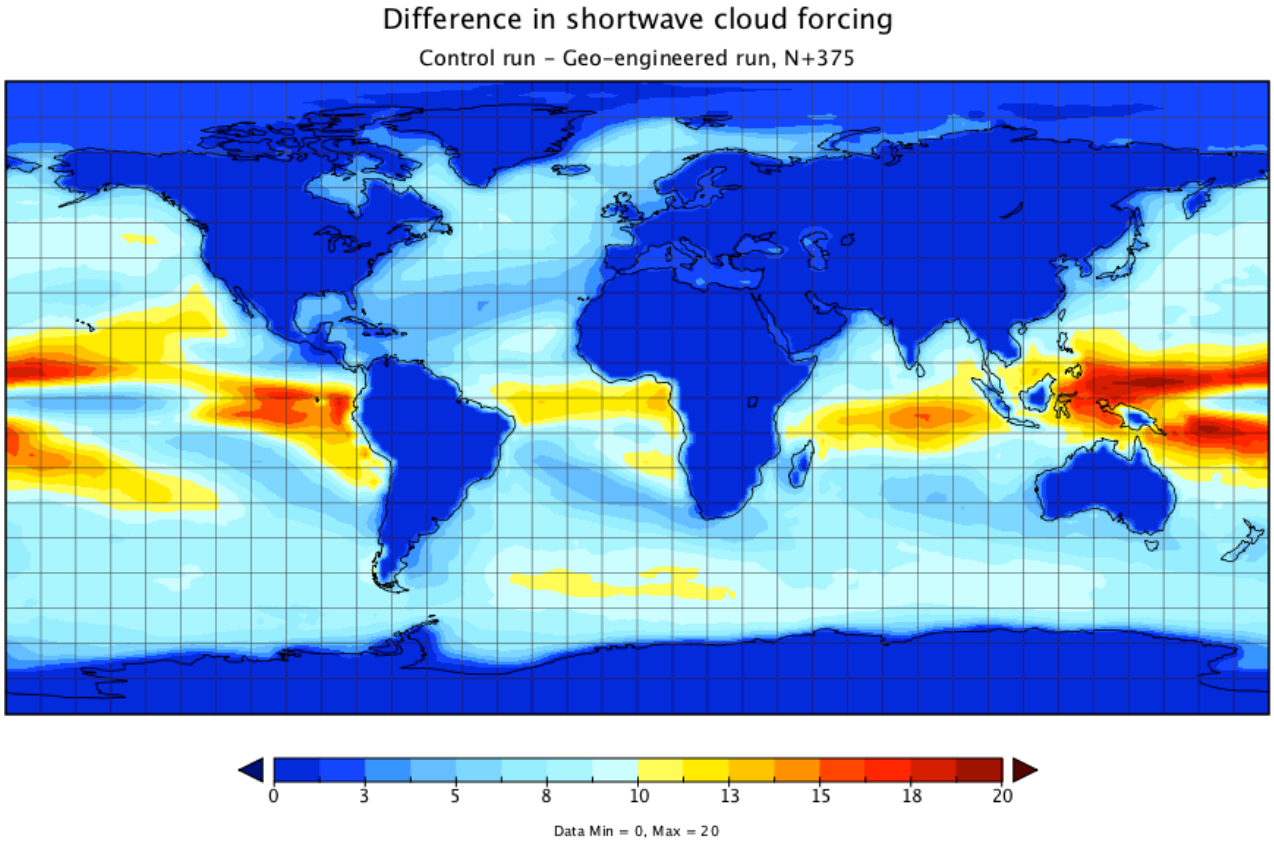

Figure 4.17: Zonally averaged CDNC, cm^{-3}

4.4 Geoengineering run, N= 375

By setting CDNC over ocean to a fixed value of 375 cm^{-3} natural variability of CDNC is somewhat restricted. The CDNC is rather altered from the previous runs, since the final CDNC is now uniform over open ocean. The difference in values from the control run is now elusively based on the control run. The zonal averages still shows a lag of CDNC increases in the Northern Hemisphere, but not nearly as much as in some previous analysis of data in this study.

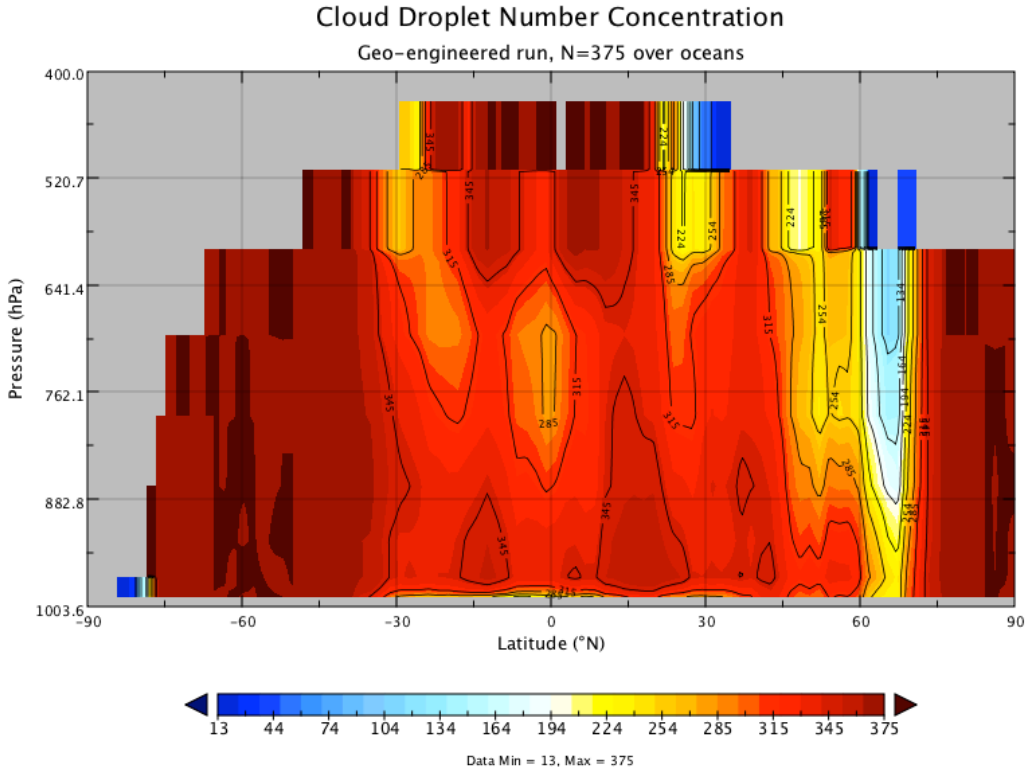

Figure 4.18: Zonally averaged CDNC, cm^{-3}

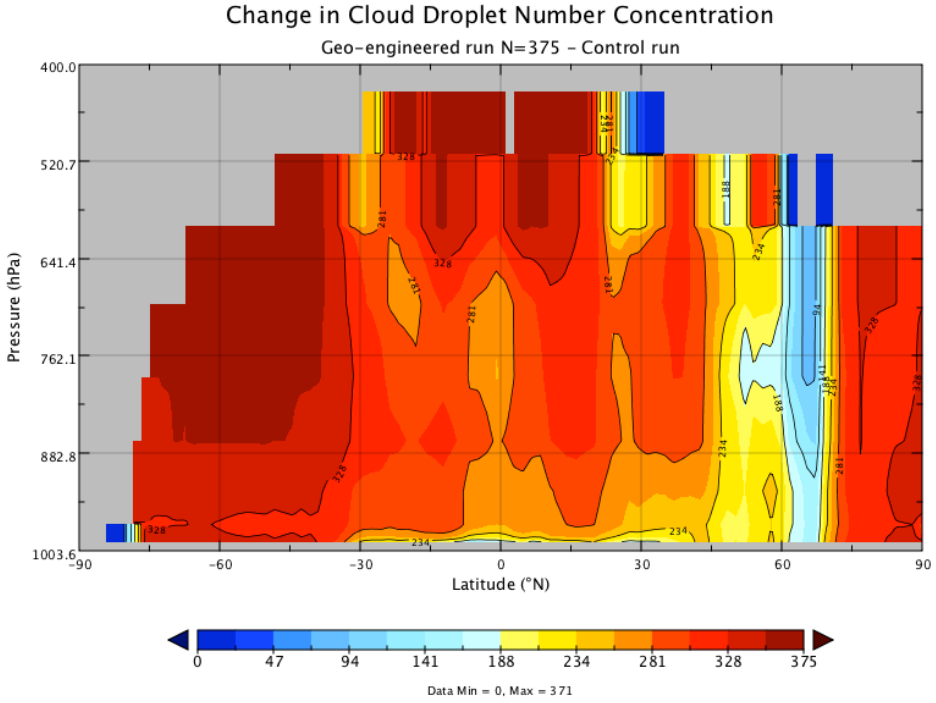

Figure 4.19: Zonally averaged change in CDNC, cm^{-3}

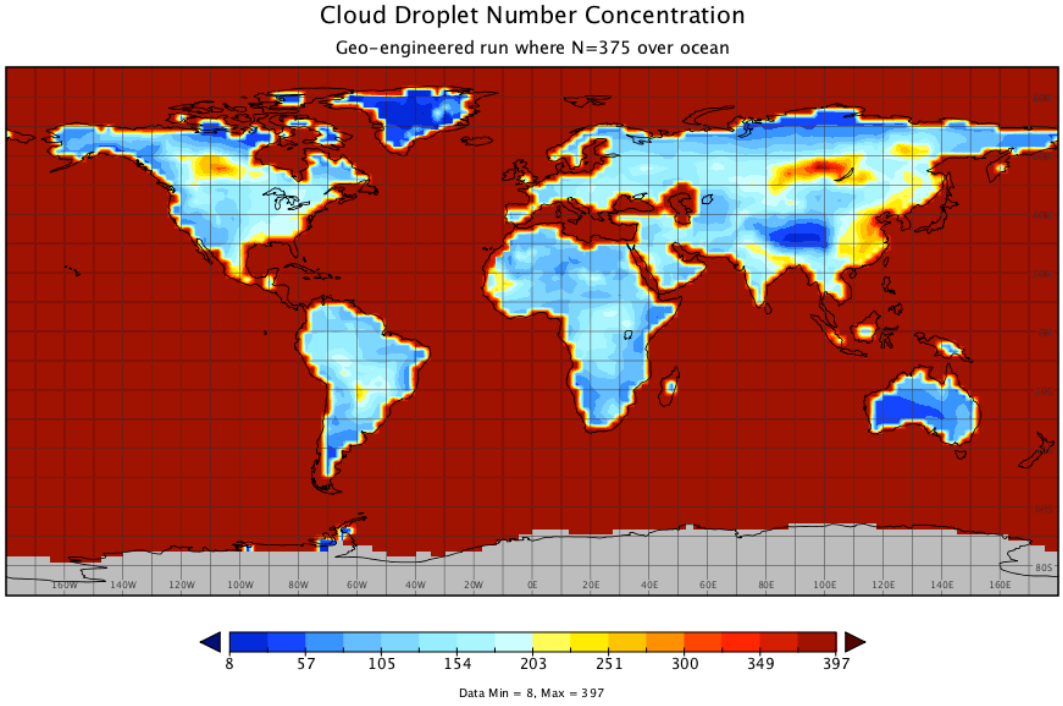

Figure 4.20: CDNC, cm^{-3}

Global distribution of the CDNC at about 930 hPa is shown in figure 4.24 and the SWCF distribution is depicted in figure 4.21

The SWCF for this case is -50.56 W/m^{-2}, figure 4.21. The difference from the control run is -5,17 W/m^2. With the fixed value of CDNC over ocean does not affect the pattern of the SWCF very much. With the CDNC fixed some areas over ocean experience less CDNC than in the previous run, CDNC+375. Figure 4.22 reveals the pattern of the change in SWCF to be much the same as before.

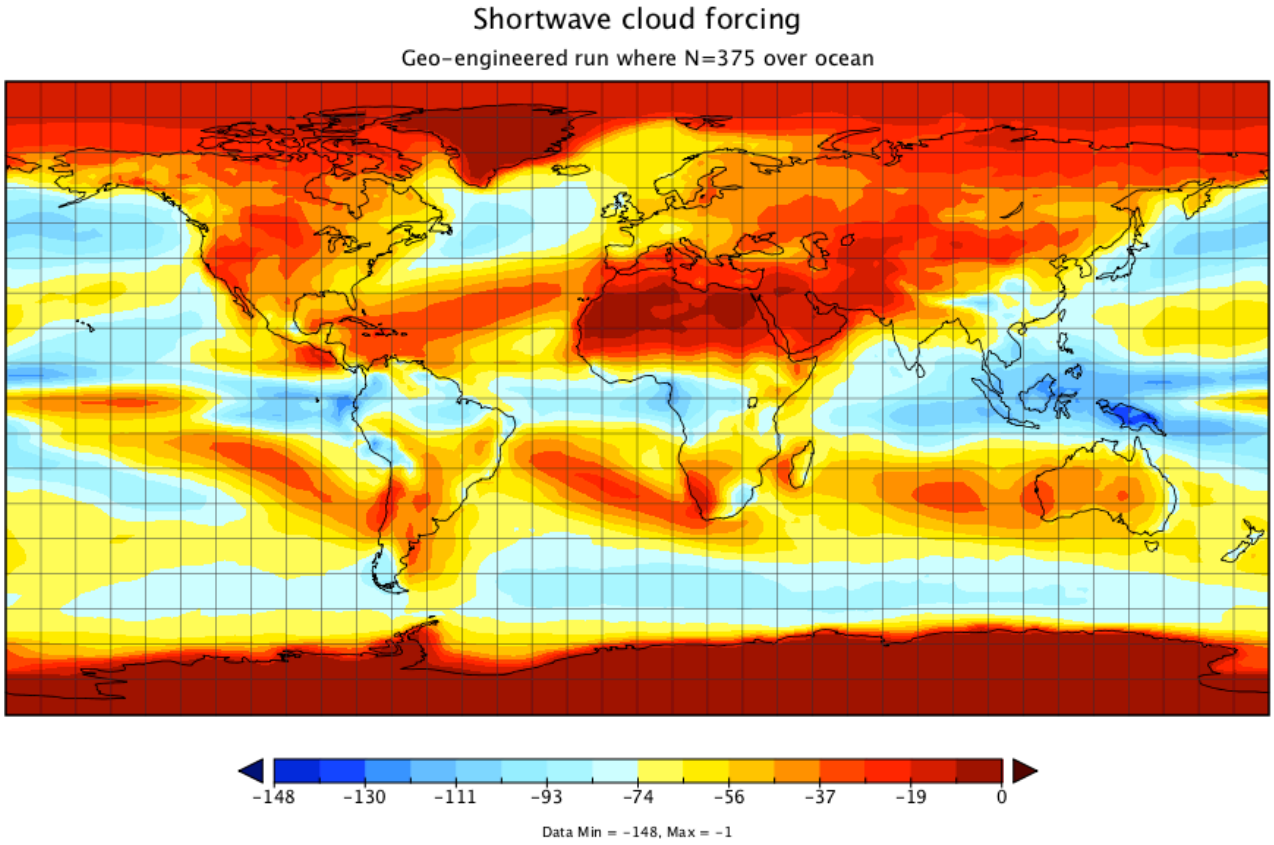

Figure 4.21: Short wave cloud forcing, W/m^2

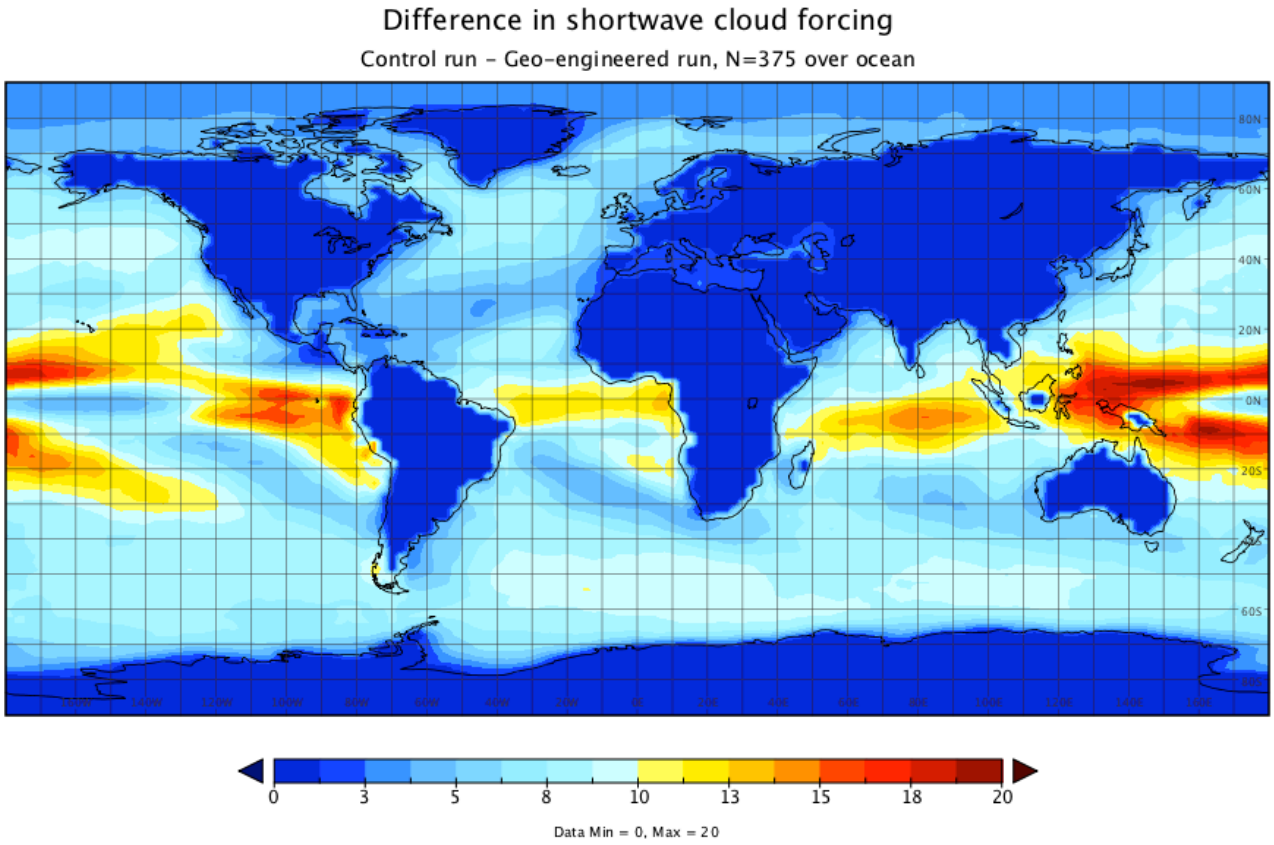

Figure 4.22: Difference in short wave cloud forcing, W/m^2

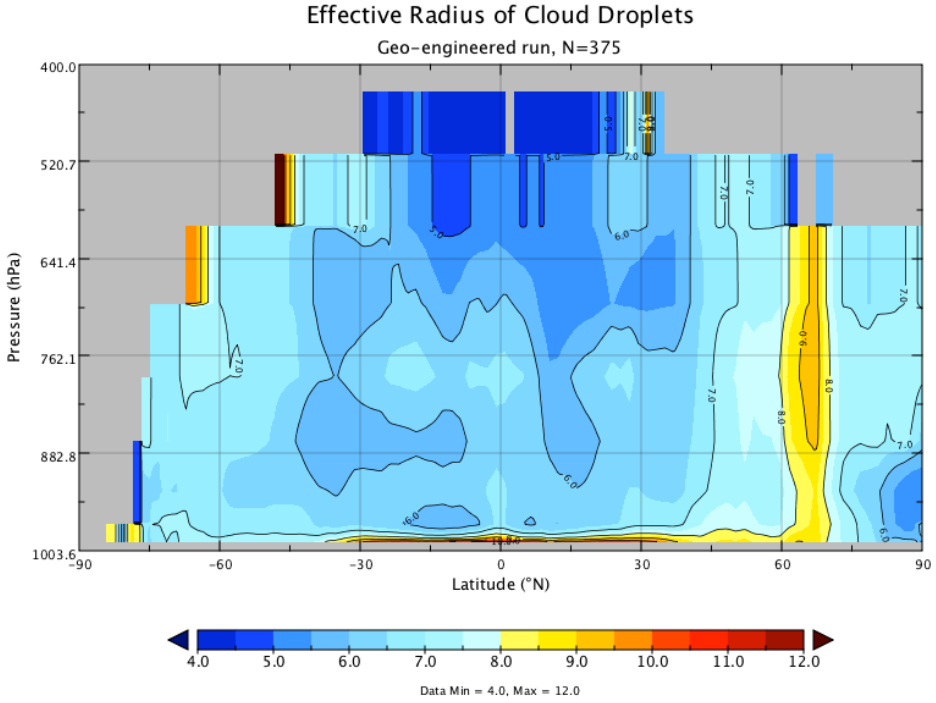

Figure 4.23: Zonally averaged effective droplet radius μm

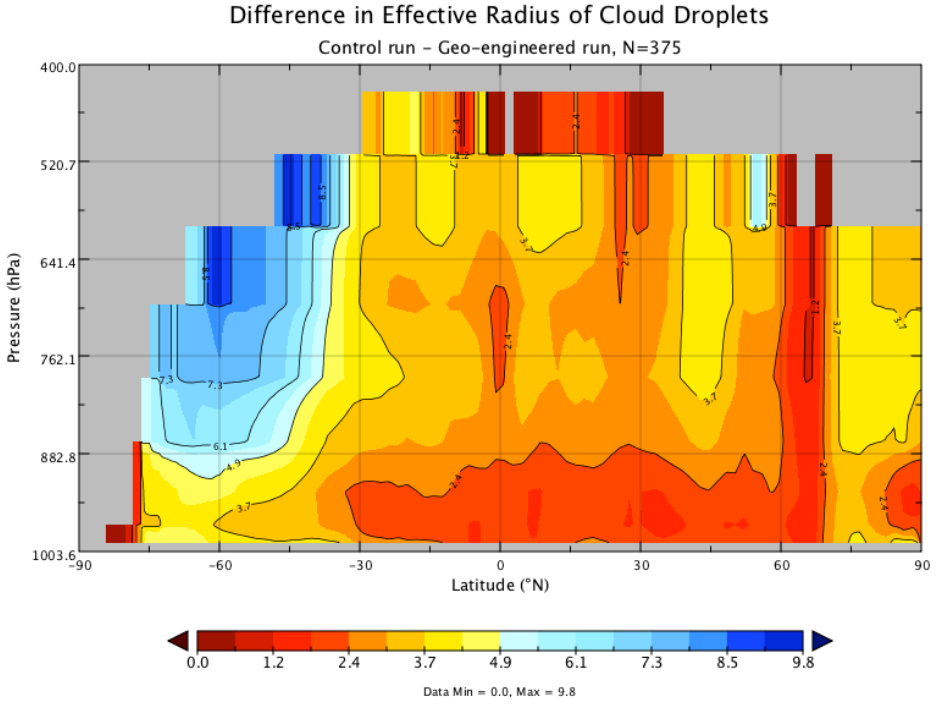

Figure 4.24: Zonally averaged difference in effective droplet radius μm

Chapter 5

Summary

In this study geo-engineered simulations of clouds with increased CDNC were carried out and compared to a control run which simulates the climate as it is. The aim was to discover if increased CDNC in low clouds over ocean would strengthen the shortwave cloud forcing and thus produce a cooling effect on the planet. This is done in effort to ameliorate the ongoing and predicted global warming. Main results show that with increased CDNC the SWCF strengthens, and while the increase of CDNC needst to be much greater than 50 cm^{-3} to counteract the 3.7 W/m^2 produced by greenhouse radiative forcing the effects would still produce cooling effects equivalent to SWCF = -2,46 W/m2.

The CDNC+375 as well as CDNC=375 over ocean both resulted in enough strengthening in the SWCF to counteract the greenhouse radiative forcing. The case of CDNC=375 show similar results to [Latham et al., 2008], where as the CDNC+375 case showed only slightly lower values, but has to be considered more realistic for practical purposes.

Geo-engineering is a young discipline and there are too many factors unknown for scientists to start in-situ experiments as is, but with the since the one of the largest problems facing the world today is the problem of global climate change there is definitely a reason to keep the research going.

Bibliography

Bruce A. Albrecht. Aerosols, cloud microphysics and fractional cloudiness. *Nature*, 1245(4923):1227–1230, September 1989.

K. Alterskjaer, J.E. Kristjansson, and O. Seland. Response of the climate system to aerosol direct and indirect forcing: Role of cloud feedbacks. *Atmos. Chem. Phys.*, 12:2795–2807, 2012. doi: 10.5194/acp-12-2795-2012.

R. Angel. Feasibility of cooling the earth with a cloud of small spacecraft neat the inner lagrange point (l1). *Proc. of the National Academy of Sciences*, 103: 17184–17189, 2006.

B.P. Briegleb. Delta-eddington approximation for solar radiation in the ncar community climate modle. *J. Geophys. Res*, 92:7603–7612, 1992.

Robert J. Charlson, James E. Lovelock, Meinrat O. Andreae, and Stephen G. Warren. Oceanic pythoplankton, atmospheric sulphur, cloud albedo and climate. *Nature*, 326:655–661, 1987. doi: doi:10.1038/326655a0.

J.G. Charney, R. Fj́ortoft, and J. von Neumann. Numerical integration of the barotropic vorticity equation. *Tellus*, 2:237–254, 1950. doi: 10.1111/j.2153.1950.tb00336.x.

P. J. Crutzen. Albedo enhancement by stratospheric sulphur injections: a contribution to resolve a policy dilemma? *Climatic Change*, 77:211–220, 2006. doi: 10.1007/s10584-006-9101-y.

Peter. R. Grent, Gokhan Danabasoglu, Leo J. Donner, Marika M. Holland, Elizabeth C. Hunke, Steve R. Jayne, David M. Lawrence, Richard B. Neale, Philip J. Rasch, Mariana Vertenstein, Patrick H Worley, Zong-Liang Yang, and Minghua Zhang. The community climate system model version 4. *Journal of Climate*, 24, October 2011. doi: 10.1175/2011JCLI4083.1.

Dennis L. Hartmann. *Global Physical Climatology*, volume 56 of *International Geophysics Series*. Academic Press, 1994.

C. Hoose, J.E. Kristjansson, Trond Iversen, Alf Kirkevag, O. Seland, and A. Gettelmann. Constraining cloud droplet number concentration in gcms suppresses the aerosol indirect effect. *J. Geophys. Res.Lett*, 65:LI2807, 2009. doi: 10.1029/2009GL038568.

Robert A. Houze. *Cloud Dynamics*, volume 53 of *International Geophysics Series*. Academic Press, 1993.

Andy Jones, John Latham, and Michael H. Smith. Radiative forcing due to modifications of marine stratocumulus clouds. *Atm. Sci. Lett.*, 2005.

Andy Jones, Jim Haywood, and Olivier Boucher. Climate impacts of geoengineering marine straocumulus clouds. *J. Geophys. Res.*, 114(D10106), 2009. doi: 10.1029/2008JD011450.

J. Kristiansen and J.E. Kristjansson. Shortwave cloud forcing of marine stratocumulus clouds. *Phys. Chem. Earth. (B)*, 24(3):225–230, 1999.

J. E. Kristjansson, X. Rasmussen, T. Iversen, A. Kirkevag, and O. Seland. Sensitivity to deliberate sea salt seeding of marine clouds - observations and model simulations. *J. Geophys. Res.*, 111(D06):D06102, 2006. doi: 10.1029/2005JD006079.

John Latham, Philip Rasch, Chin-Chieh Chen, Laura Kettles, Alan Gadian, Andrew Gettelman, Hugh Morrison, Keith Bower, and Tom Choularton. Global temperature stabilization via controlled albedo enhancement of low-level maritime clouds. *Pil. Trans. R. Soc.*, A 2008(366):3969–3987, 2008. doi: 10.1098/rsta.2008.0137.

John M. Lewis. Clarifying the dynamics of the general circulation: Phillips's 1956 experiment. *Bulletin of the American Meteorological Society*, 1998.

K.N. Liou. *An Introduction to Atmospheric Radiation, 2nd edt.*, volume 84 of *International Geophysics Series*. Academic Press, 2002.

G.A. Meehl, T.F. Stocker, W.D. Collins, P. Friedlingstein, A.T. Gaye, J.M. Gregory, A. Kitoh, R. Knutti, J.M. Murphy, A. Noda, S.C.B. Raper, I.G. Watterson, A.J. Weaver, and Z.-C. Zhao. *Global Climate Projections. In Climate Change 2007: The Physical Science Basis. Contribution of Working Group I to the Fourth Assessment Report of the Intergovernmental Panel on Climate Change, (edts:S. Solomon. and D. Qin and M. Manning and Z. Chen and M. Marquis and K.B. Averyt and M. Tignor and H.L. Miller).* Cambridge University Press, 2007.

A.A. Mirin and W.B. Sawyer. A scalable implementation of a finite-volume dynamical core in the community atmospheric mdoel. *Int'l Jour. High Performance Computing Applications*, 19(3):203, 2005.

National Academy of Science. Policy implications of greenhouse warming: Mitigation, adaptation and the science base. 1992.

Richard. B. Neale, Jadwiga H. Richter, Adnrew J. Conley, Sungsu Park, Peter H. Lauritzen, Andrew Gettelman, David Williamson, Philip J. Rash, Stephen J. Vavrus, Mark A. Taylor, William D. Collins, Minghua Zhang, and Shian-Jiann Linn. Description of the NCARCimmunity Atmosphere Model (CAM 4.0). *NCAR*, The Technical Note Series(TN-485+STR), April 2010.

J. Pearson, J. Oldson, and E. Levin. Earth rings for planetary environment control. *Acta Astronautica*, 58:45–57, 2006.

V. Ramanathan, R.D. Cess, E.F. Harrison, P. Minis, B.R. Barkstrom, E. Ahmad, and D. Hartmann. Cloud-radiative forcing and climate: Results from the earth radiation budget experiment. *Science*, 243(4887):57–63, 1989.

V. Ramaswamy, O. Boucher, J. Haigh, D. Hauglustaine, J. Haywood, G. Myhre, T. Nakajima, G. Y. Shi, and S. Solomon. *Radiative forcing of climate change. In Climate Change, 2001: the Scientific Basis. Contribution of working group I to the third assessment report of the intergovernmental panel on climate change. (edts. J.T. Haughton and Y. Ding and D. J. Griggs and M. Nouger and P.J. van der Linden and X. Dai and K. Maskell and C.A. Johnson).* Cambridge University Press, 2001.

Philip J. Rasch, John Latham, and Chih-Chich (Kack) Chen. Geoengineering by cloud seeding: influence on sea ice and climate system. *Env. Res. Lett.*, 4 (045112), 2009. doi: 10.1088/1748-9325/4/4/045112.

P.J. Rasch and J.E. Kristjánsson. A comparison of the ccm3 model climate using diagnosed and predicted condensate parameterization. *Journal of Climate*, 11: 1587–1614, 1998.

R.R. Rogers and M.K. Yau. *A Short Course in Cloud Physics*, volume 113 of *International Series in Natural Philosophy*. Butterworth -Heinemann, 1989.

Hauke Schmidt, Asbjorn Aaheim, Jon-Egill Kristjansson, Mark ő̈awrence, Michael Schulz, and Claudia Timmreck. Statement on geoengineering, its potential uses, costs and side effects, December 2008. URL `http://implicc.zmaw.de/Science.671.0.html`.

O. Seland, T. Iversen, A. Kirkevag, and T. Storelvmo. Aerosol-climate interactions in the CAM-Oslo atmospheric GCM and investigation of associated basic shortcomings. *Tellus*, 60A:459–491, 2008.

A. Slingo. Sensitivity of the earth's radiation budget to changes in low clouds. *Nature*, 343(6253):49–51, Jan 1990.

Trude Storelvmo, Jon Egill Kristjansson, Steven J. Ghan, Alf Kirkevag, O. Seland, and Trond Iversen. Predicting cloud droplet number concentration in Community A tmosphere model (CAM)-Oslo. *J. Geophys. Res.*, 111:D24208, 2006. doi: 10.1029/2005JD00630.

Trude Storelvmo, Jon Egill Kristjansson, and Ulrike Lohmann. Aerosol influence on mixed-phase clouds in cam-oslo. *Journal of the Atmospheric Sciences*, 65: 3214–3230, 2008. doi: 10.1175/2008JAS2430.1.

The Royal Society. Geoengineering the climate; science, governance and uncertainty. *RS Policy Document*, 10/09(RS1636), September 2009.

T.M. Lenton and N. E. Vaughan. The radiative forcing potential of different climate geoengineering options. *Atmos. Chem. Phys.*, 9:5539–5561, 2009.

S. Twomey. The influence of pollution on the shortwave albedo of clouds. *J. Atmos. Sciences*, 34, 1977.